

# Moist Absolute Instability: The Sixth Static Stability State



George H. Bryan and J. Michael Fritsch

Department of Meteorology, The Pennsylvania State University, University Park, Pennsylvania

## ABSTRACT

It is argued that a sixth static stability state, moist absolute instability, can be created and maintained over mesoscale areas of the atmosphere. Examination of over 130 000 soundings and a numerical simulation of an observed event are employed to support the arguments in favor of the existence of moist absolutely unstable layers (MAULs).

Although MAULs were found in many different synoptic environments, of particular interest in the present study are the deep ( $\geq 100$  mb) layers that occur in conjunction with mesoscale convective systems (MCSs). A conceptual model is proposed to explain how moist absolute instability is created and maintained as MCSs develop. The conceptual model states that strong, *mesoscale, nonbuoyancy*-driven ascent brings a conditionally unstable environmental layer to saturation faster than small-scale, buoyancy-driven convective elements are able to overturn and remove the unstable state. Moreover, since lifting of a moist absolutely unstable layer *warms* the environment, the temperature difference between the environment and vertically displaced parcels is reduced, thereby decreasing the buoyancy of convective parcels and helping to maintain the moist absolutely unstable layer.

Output from a high-resolution numerical simulation of an event exhibiting this unstable structure supports the conceptual model. In particular, the model indicates that MAULs can exist for periods greater than 30 min over horizontal scales up to hundreds of kilometers along the axis of the convective region of MCSs, and tens of kilometers across the convective region.

The existence of moist absolute instability suggests that some MCSs are best characterized as slabs of saturated, turbulent flow rather than a collection of discrete cumulonimbus clouds separated by subsaturated areas. The processes in MAULs also help to explain how an initially unsaturated, stably stratified, midlevel environment is transformed into the mesoscale area of saturated moist-neutral conditions commonly observed in the stratiform region of mesoscale convective systems.

## 1. Introduction

Static stability considers the temperature of a displaced parcel relative to the environmental temperature surrounding the parcel. Traditionally, five static stability states are recognized (Saucier 1955; Hess 1959):

- |                      |                       |
|----------------------|-----------------------|
| 1) absolutely stable | $\gamma < \Gamma_s$ , |
| 2) saturated neutral | $\gamma = \Gamma_s$ , |

- |                            |                                  |
|----------------------------|----------------------------------|
| 3) conditionally unstable  | $\Gamma_s < \gamma < \Gamma_d$ , |
| 4) dry neutral             | $\gamma = \Gamma_d$ ,            |
| 5) dry absolutely unstable | $\gamma > \Gamma_d$ ,            |

where  $\gamma$  is the observed environmental lapse rate, and  $\Gamma_s$  and  $\Gamma_d$  are the moist- and dry-adiabatic lapse rates, respectively. Of particular interest here is state 5, dry absolutely unstable. Typically, this state exists in a shallow surface-based layer (usually  $< 100$  mb deep) and results from an imbalance between the rate at which air adjacent to the ground is heated by conduction and the rate at which dry convective eddies (restricted to dry-adiabatic overturning) can transport the heated air upward (Hodge 1956; Slonaker et al. 1996). It is most often observed on clear dry days when surface heating by incoming shortwave radiation is intense. Under these conditions, dry convective eddies

---

Corresponding author address: George H. Bryan, 503 Walker Building, University Park, PA 16802.

E-mail: bryan@essc.psu.edu

In final form 22 October 1999.

©2000 American Meteorological Society

are unable to transport heat upward fast enough to maintain the dry-adiabatic lapse rate. In other words, the absolutely unstable state is simply a manifestation of a rate imbalance wherein the large-scale radiative processes acting to destabilize the atmosphere exceed the small-scale convective processes acting to stabilize. In principle then, the absolutely unstable state can be maintained as long as the rate imbalance continues, and can exist over areas much larger than the scale of individual convective eddies.

In view of the fact that nature is able to create and maintain a dry absolutely unstable state, it is conceivable then that there may be a sixth stability state where a *saturated lapse rate* ( $\gamma_s$ ) that is steeper than the moist-adiabatic lapse rate can be created and maintained, that is,

$$6) \text{ moist absolutely unstable } \quad \gamma_s > \Gamma_s.$$

Although Saucier (1955) and Hess (1959) do not preclude the existence of a saturated lapse rate that is unstable, they do not specifically mention the criteria for moist absolutely unstable conditions, nor has it been explained how this structure is created or removed. Furthermore, the temporal and spatial scales of moist absolutely unstable conditions has never been explored.

The claim that moist absolute instability can be created *and maintained* flies counter to the accepted view that moist, fast-growing, nonhydrostatic modes (e.g., convective clouds/thunderstorms) will ensue immediately following saturation (if the lapse rate is steeper than moist adiabatic) and that the unstable state will be quickly eliminated or neutralized (e.g., Bjerknes 1938; Lilly 1960). However, this conven-

tional view does not take into account the rate at which processes may be creating the unstable state, or the rate at which processes remove the unstable state. In other words, as with the creation of the dry-superadiabatic layer, *it may be possible that a moist absolutely unstable state can be created faster than (moist) convective turbulence can eliminate it.*

It is important to note here that moist absolute instability is not equivalent to conditional instability.<sup>1</sup> In a typical conditionally unstable situation, the environment is unsaturated and an initially unsaturated *parcel* is lifted to saturation [i.e., raised to its lifted condensation level (LCL)]. Further lifting of the parcel along a moist adiabat *sometimes* results in the saturated parcel becoming warmer than its environment. If this occurs, nonhydrostatic buoyancy-driven vertical accelerations support continued upward displacement of the parcel; that is, upward displacement of the parcel is unstable. However, this is not always the case. For example, the entire sounding shown in Fig. 1a is conditionally unstable. For parcels originating below 900 mb, further lift above the LCL can eventually result in positive accelerations. On the other hand, parcels originating from above 850 mb never become positively buoyant.

Consider now the moist absolutely unstable condition that results if the entire lower troposphere, as

<sup>1</sup>The term “conditional instability” in this paper is defined by static stability state 3 (following Saucier 1955 and Hess 1959). Sometimes, conditional instability is used to describe a sounding that contains a *parcel* that can become positively buoyant after being lifted to its lifted condensation level and then to its level of free convection. Emanuel (1997) has proposed the term “metastability” to describe this latter state.

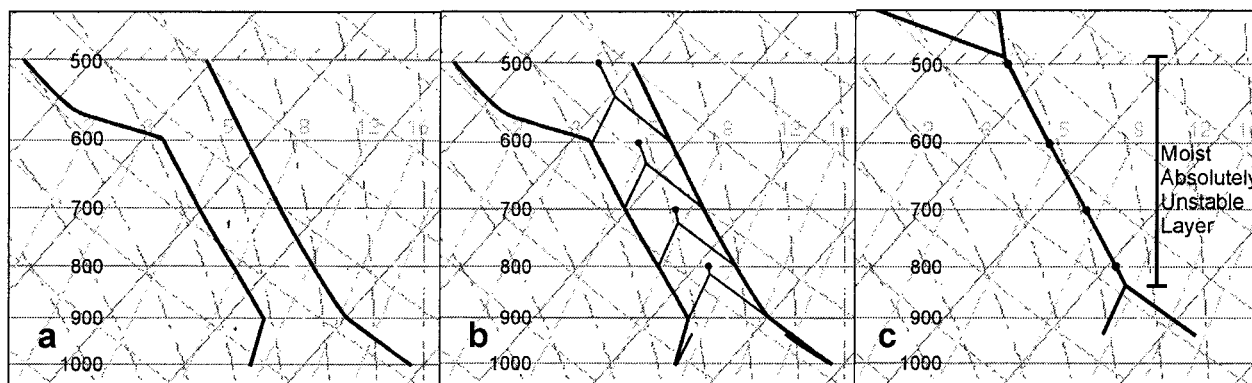


FIG. 1. Idealized sounding: (a) initial conditionally unstable sounding, (b) layer lifting is applied (thin black lines represent the path of selected parcels within the lifted layer), and (c) resulting structure after lifting, which features a deep moist absolutely unstable layer.

depicted in Fig. 1a, is lifted to saturation (Figs. 1b,c). All parcels in the saturated layer of Fig. 1c are unstable to any displacement in either direction, up or down.<sup>2</sup> Thus, as its name implies, the layer in Fig. 1c is inherently unstable. Intuitively, it would seem that this structure could not be maintained as a separate stability state. However, evidence exists that moist absolutely unstable layers over 100 mb deep do develop (Kain and Fritsch 1998). In fact, Kain and Fritsch argued that this unstable state can extend several hundred kilometers in the horizontal and can persist for time periods longer than the lifetime of moist convective turbulence (i.e., cumulus clouds). These conditions can often occur at the inflow region of mesoscale convective systems, where a deep layer of strong mesoscale ascent extends for tens to hundreds of kilometers.

The goal of this paper is to establish that a sixth stability state, moist absolute instability, is sometimes present in the low to midtroposphere. The consequences of this state on the structure of mesoscale convective systems are also explored. To this end, observations from the standard radiosonde network are presented in section 2. A conceptual model for the creation and maintenance of moist absolutely unstable layers is proposed in section 3. The results from a non-hydrostatic cloud-scale-resolution numerical simulation of an event with moist absolute instability are examined in section 4. The implications of this state on the structure and organization of mesoscale convective systems are discussed in section 5. A summary and concluding remarks are provided in the final two sections.

## 2. Rawinsonde observations

Data from the standard rawinsonde network in the United States was examined to see if moist absolutely unstable layers (MAULs) are observed. Data from the 72 rawinsonde sites in the continental United States from 1 January 1997 to 31 August 1999 were analyzed.

<sup>2</sup>An unstable downward displacement does require, however, access to water condensate in order to maintain saturation or near-saturation during its descent.

Soundings from nonstandard release times (e.g., not released at 0000 UTC or 1200 UTC) were included in the study. Only the mandatory and significant level data were available.

A sounding was considered to have a MAUL if it contained a saturated layer in which the equivalent potential temperature ( $\theta_e$ ) decreased with height. The definition of  $\theta_e$  recommended by Bolton (1980) was used. Saturation was defined as a dewpoint depression of  $\leq 1^\circ\text{C}$ . This criterion for saturation was chosen because of the reported accuracy of radiosonde humidity sensors ( $0.2^\circ\text{--}0.5^\circ\text{C}$ ; WMO 1996) and because of the typical dry bias at high relative humidity (Schmidlin 1998).

Results of this investigation confirmed the existence of MAULs. Table 1 lists some properties of the MAULs that were identified. A surprising 24.1% of the 134 196 soundings had layers that fit the criteria listed above. However, most of these layers were only slightly greater than moist adiabatic and were shallow (a few tens of millibars deep). Soundings with MAULs that are deep ( $\geq 100$  mb) and with relatively strong lapse rates [ $\partial\theta_e/\partial z \leq -3 \text{ K km}^{-1}$ ] composed 1.1% of the dataset, which is an average of 1.5 deep, intense MAULs every day in the continental United States rawinsonde network. Although MAULs were found in every month of the study, there was a greater tendency for MAULs to be found in summer months.

It is important to recognize that not all of the MAULs reported by rawinsonde ascents are physically realistic. There are several ways in which apparent (but unrealistic) MAULs can appear in rawinsonde ascents, including

TABLE 1. Properties of the moist absolutely unstable layers (MAULs) in the rawinsonde study.

	Number/percent of total soundings	Depth (mb) mean/median	$\partial\theta_e/\partial z$ ( $\text{K km}^{-1}$ ) mean/median
All MAULs	32 407/24.1%	40.3/29.4	-6.29/-3.22
MAULs with depth $\geq 100$ mb	3281/2.4%	140.4/128.0	-3.30/-2.60
MAULs with $\partial\theta_e/\partial z \leq -3 \text{ K km}^{-1}$	18 866/14.1%	35.9/25.0	-10.76/-6.56
MAULs with depth $\geq 100$ mb and $\partial\theta_e/\partial z \leq -3 \text{ K km}^{-1}$	1433/1.1%	138.8/127.0	-5.60/-4.82

- instrument error,
- wet or ice-covered humidity sensors in a rawinsonde package that continue reporting saturated conditions after leaving clouds, and
- rapid horizontal advection of a balloon-borne sounding through a saturated environment with a strong horizontal temperature gradient.

Furthermore, humidity chamber tests have shown that radiosonde humidity sensors can lose accuracy after saturation is reached (Blackmore and Taubvurtzel 1999). These problems suggest that many of the MAULs identified in the standard rawinsonde data are not realistic. However, it is reasonable to assume that *some* of the 1433 deep, intense MAULs that were identified *are* physically realistic.

Examination of soundings that contain MAULs together with the environment they sampled would help answer the question of whether MAULs are physically realistic. An informal investigation was conducted in the April–August period of 1997–98 to gain insight into the environments in which MAULs were observed. Soundings east of the Rockies were examined if they sampled the near environment of moist convection. All events with radar reflectivity  $\geq 40$  dBZ (based upon the national network of WSR-88D radars) within 100 km of a sounding site and within 1 h of a sounding release time (i.e., between 1000 and 1200 UTC and 2200 and 0000 UTC) were examined on a “time available basis”; that is, there was no automated routine for obtaining data. MAUL events that were identified in this informal investigation indicate that nearly all deep MAULs occurred in proximity to moist convection (i.e., thunderstorms, mesoscale convective systems, or stratocumulus layers). The fact that MAULs were found in both deep precipitating convection and shallow nonprecipitation convection suggests that MAULs can be created and maintained by different processes.

It is interesting to note that many of the MAUL soundings were observed in close proximity to the zone where the inflow to mesoscale convective systems (MCSs) was being lifted by the MCS’s moist-downdraft outflow. In these cases, the MCS outflow boundary typically was within a few tens of kilometers of the sounding site, suggesting that MAULs are only a few tens of kilometers wide. Thus, there appears to be only a small window of opportunity to observe MAULs with rawinsondes. Our search for MAULs in the United States rawinsonde network in 1997 and 1998 revealed two additional factors that reduced the

likelihood of observing MAULs: 1) the odds that the outflow boundary of a mature MCS was near a sounding site at sounding-release time are exceedingly small, and 2) when conditions are ripe to sample a MAUL, they are not ideal conditions for the release of a rawinsonde (it is quite likely that some rawinsonde operators were unable or unwilling to release the balloon in instances where heavy rainfall and lightning were approaching). Considering all of the above factors, it is not at all surprising that MAULs would go unnoticed or that the existence of such a state would be viewed with great skepticism.

### 3. Saturated absolute instability in mesoscale convective systems

The remainder of this paper promotes a conceptual model for saturated absolute instability that is observed in the inflow regions of mesoscale convective systems. Some conceptual models of moist convective overturning in MCSs depict an ensemble of individual convective towers (in various stages of development and decay) emanating from a well-mixed convective boundary layer (e.g., Arakawa and Schubert 1974). These models fit the theoretically supported view that, in the presence of a deep conditionally unstable state, moist convective overturning will be dominated by fast-growing nonhydrostatic modes, that is, thunderstorms. However, following the early work of Moncrieff and Green (1972), Betts et al. (1976), Zipser (1977), Houze (1977), Ogura and Chen (1977), and LeMone et al. (1984), a wealth of evidence (Table 2) has been compiled showing that, under certain conditions, the atmosphere convectively overturns in a manner more resembling mesoscale slabs (or sheets) of ascending air overrunning slabs of descending air. These slabs are typically several hundred kilometers wide in the cross-flow direction and a few tens to several hundred kilometers long in the along-flow direction (e.g., Roux et al. 1984; Chong et al. 1987; Smull and Augustine 1993; Trier and Parsons 1993). Types of MCSs exhibiting slab overturning include certain squall lines, elevated convection events, and narrow cold frontal rainbands.

Typically, ascending slabs develop along elongated swaths of strong dynamic<sup>3</sup> lifting, such as that found

<sup>3</sup>The term “dynamic lifting,” as used here and elsewhere in the paper, refers to vertical motions *not* generated by buoyancy-driven acceleration.

along surface-based outflow layers, along frontal zones, or possibly by the release of moist symmetric instability. Dual-Doppler radar analyses suggest that, in some instances, dynamically driven ascent of several meters per second develops in a low-level layer several kilometers deep and that this rapidly ascending layer may extend horizontally for over 100 km. For example, Fig. 2a shows a vertical cross section perpendicular to a convective line observed during PRE-STORM (Smull and Augustine 1993). Low-level inflow of high  $\theta_e$  air is directed from right to left and is being forced upward by outflow from a surface-based cold pool. Note the low-level vertical motion maximum of  $10 \text{ m s}^{-1}$  centered near 3.5 km; this low-level maximum is clearly distinct from a stronger maximum, presumably driven by buoyancy, centered near 10.5 km. Analyses of other MCSs also show two distinct maxima in ascent located at similar elevations (e.g., Biggerstaff and Houze 1993; Hildebrand et al. 1996; Kingsmill and Houze 1999). Figure 2b shows a horizontal plot of Doppler-derived vertical motion at 1.0 km above ground for a MCS observed during COPT 81 (Chong et al. 1987). Low-level inflow for this system, which is directed from left to right, is forced strongly upward along the outflow boundary; in this region, ascent reaches magnitudes of  $3\text{--}6 \text{ m s}^{-1}$ . The dual-Doppler analysis region of Fig. 2b shows a 30-km long swath of uninterrupted ascent, but the low-level reflectivity image (not shown) suggests that this swath of ascent is over 80 km long. This example of a continuous low-level swath of strong ascending motion is in sharp contrast to a collection of cumulonimbus updrafts

where only a small percent of the environmental area is composed of updrafts. In other words, the entire low-level mesoscale environment is ascending as opposed to ascent only in individual cumulonimbus updrafts (which can emerge from the slab at mid and upper levels).

Observed by radar, this slab convective overturning often appears as a mesoscale zone of contiguous echo that may extend for hundreds of kilometers (e.g., Figs. 3a,b). A swath of strong echo, called the “convective region” of mesoscale convective systems (e.g., Houze et al. 1989; Loehrer and Johnson 1995), is often found along the inflow side, paralleling a front or outflow boundary. As documented by Houze et al. (1990) and McAnelly and Cotton (1986), there is considerable variation in small-scale structure within the convective regions of mesoscale convective systems. For example, the convective region in Fig. 3a shows a virtually solid swath of reflectivity values  $> 40 \text{ dBZ}$  at the leading edge of the slab, while the convective region in Fig. 3b shows a line of discrete convective cells embedded within a nearly unbroken swath of slightly weaker reflectivities. The individual cells of Fig. 3b resemble and are similar in scale to the traditional models of distinct “hot towers” and would be considered individually as thunderstorms. In other instances, the number of these embedded cells is much greater, however their size is much smaller. In a very detailed and careful analysis of an MCS, Yuter and Houze (1995a,b) found a broad-size distribution of cellular elements in the convective region.

The long solid swaths of strong moist ascent, such as shown in Fig. 3a, produce copious electrical activ-

TABLE 2. Papers supporting the occurrence of slab overturning.

Newton (1950)	Heymsfield and Schotz (1985)	Houze et al. (1989)
Fujita (1955)	Smull and Houze (1985)	Moncrieff (1989)
Newton and Newton (1959)	Leary and Rappaport (1987)	Zhang et al. (1989)
Houze (1977)	Chong et al. (1987)	LeMone and Jorgensen (1991)
Ogura and Chen (1977)	Dudhia et al. (1987)	Frankhauser et al. (1992)
Zipser (1977)	Smull and Houze (1987)	Smull and Augustine (1993)
Leary and Houze (1979)	Chalon et al. (1988)	Trier and Parsons (1993)
Ogura and Liou (1980)	Fovell and Ogura (1988)	Lemone and Moncrieff (1994)
Moncrieff (1981)	Lafore et al. (1988)	Skamarock et al. (1994)
Thorpe et al. (1982)	Rotunno et al. (1988)	Yuter and Houze (1995)
Gamache and Houze (1982)	Roux (1988)	Pandya and Durran (1996)
Maddox (1983)	Weisman et al. (1988)	Jorsensen et al. (1997)
Roux et al. (1984)	Cotton et al. (1989)	Kain and Fritsch (1998)

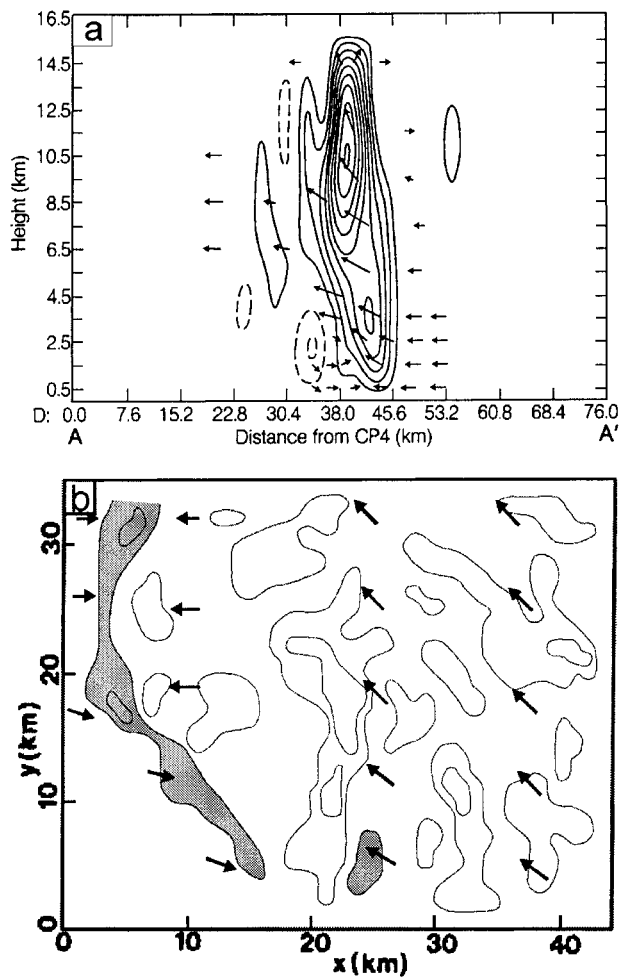


FIG. 2. Dual-Doppler radar observations of mesoscale convective systems. (a) Cross section of vertical velocity ( $w$ , contour interval is  $2 \text{ m s}^{-1}$ , negative contours are dashed, and zero contour is excluded). Adapted from Smull and Augustine (1993). (b) Horizontal view of  $w$  at  $1.0 \text{ km}$  above ground (shaded regions are updrafts with contours corresponding to  $+3$  and  $+6 \text{ m s}^{-1}$ , nonshaded contours are downdrafts of  $-0.5$  and  $-2 \text{ m s}^{-1}$ , and arrows indicate horizontal system-relative flow). Adapted from Chong et al. (1987).

ity but hardly fit the traditional model of “a thunderstorm” (e.g., as shown in Fig. 3c). One might ask what, exactly, should be termed a thunderstorm? Should the entire  $100\text{-km}$  long swath of high reflectivity be labeled as one thunderstorm? Colman (1990a) pointed out that thunderstorms fitting the traditional conceptual model (i.e., isolated cells) often pass between observation sites without being reported, whereas during many elevated convection events several surrounding observing sites will simultaneously report thunder. Colman proposed that these large mesoscale areas of convective precipitation are fundamentally different from the traditional concept of cumulonimbus thunderstorms. Due to the different structure of moist convective

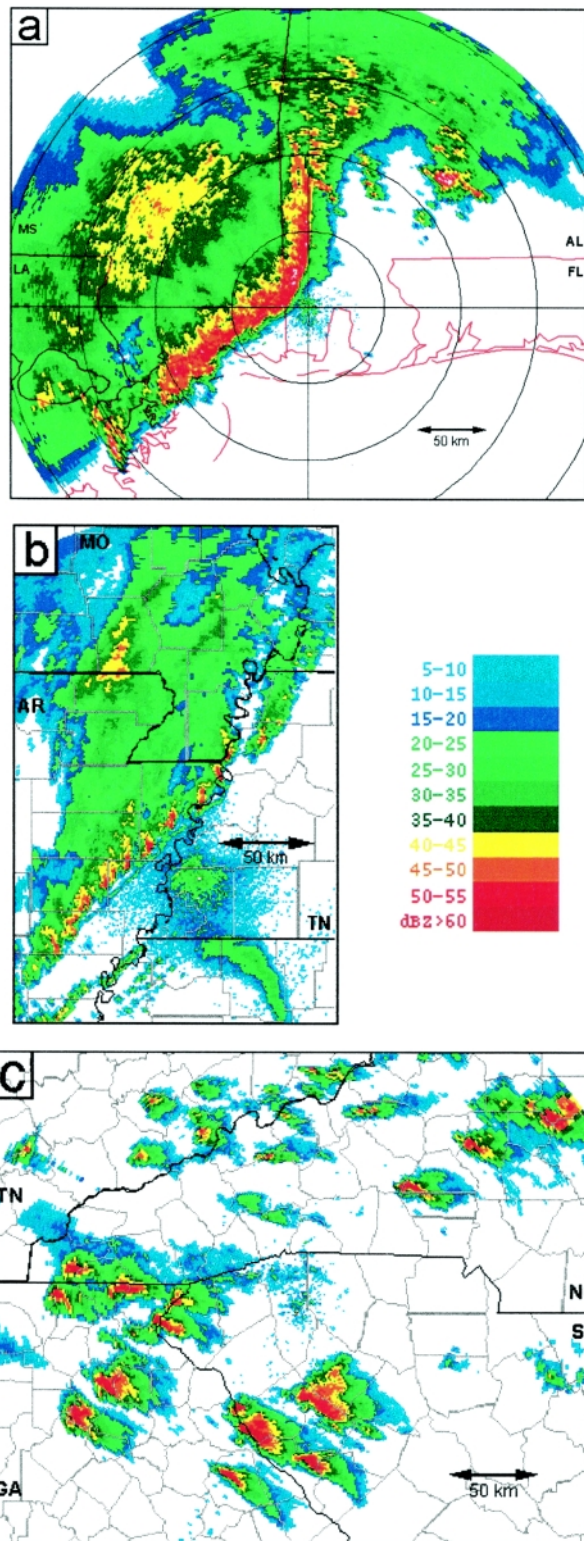


FIG. 3. WSR-88D base reflectivity images from the lowest elevation scan ( $0.5^\circ$ ): (a) Mobile, AL, 1258 UTC 22 Jan 1998; (b) Nashville, TN, 1326 UTC 22 Apr 1996; and (c) Greenville, SC, 2241 UTC 7 May 1998.

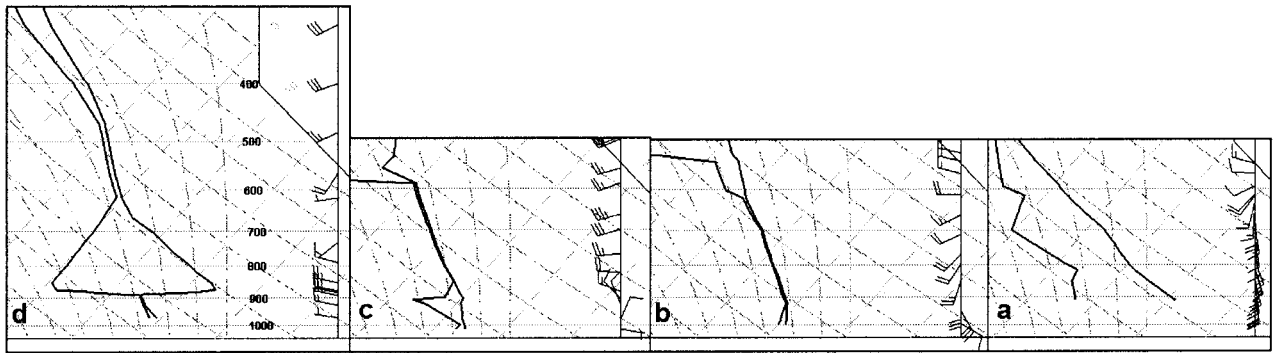


FIG. 4. Skew  $T$ -log $p$  soundings representative of the conditions at points a–d, respectively, in Fig. 5: (a) Midland, TX, 0000 UTC 12 Jun 1997; (b) Birmingham, AL, 1200 UTC 9 Aug 1997; (c) Lake Charles, LA, 1200 UTC 18 Jun 1997; and (d) Detroit, MI, 1200 UTC 21 Jun 1997.

events, and because the processes that dictate these structures are fundamentally different, we propose the terms “cellular convection” for the traditional buoyancy-driven thunderstorm model and radar signature (e.g., Fig. 3c) and “slab convection” for dynamically driven events with radar signatures like that in Fig. 3a. Note, however, that according to the definitions of Bluestein and Jain (1985) and Hane (1986), the convective regions of *both* systems would qualify as squall lines.

Naturally, the organizational differences evident in Fig. 3 raise many questions about the organization of convection. For example, what factors determine the small-scale structure within the convective region? Previous studies have identified the role of vertical wind shear, cold pool intensity, magnitude of thermodynamic instability, and the release of symmetric instability. Most relevant to this paper is that the atmosphere can create *mesoscale areas of saturation in a conditionally unstable environment*. Furthermore, these conditions do not necessarily result in a field of individual convective towers. It is within these mesoscale saturated slabs that ascent may rival the vertical motions created by buoyancy, thus creating the potential for sustained moist absolutely unstable conditions.

Figure 4 presents examples of soundings, two of which exhibit MAULs, taken at points

preceding, within, and following the convective region of MCSs. The locations of the soundings relative to the structure and circulation of an idealized MCS are shown in Fig. 5. The idealized convective system was constructed on the basis of the studies listed in Table 2. Ahead of the system, the atmosphere is conditionally unstable with a deep, well-mixed boundary layer. Parcels rising from the well-mixed layer are unable to overcome the convective inhibition and reach their level of free convection. As the outflow boundary of the convective system approaches, the environment is

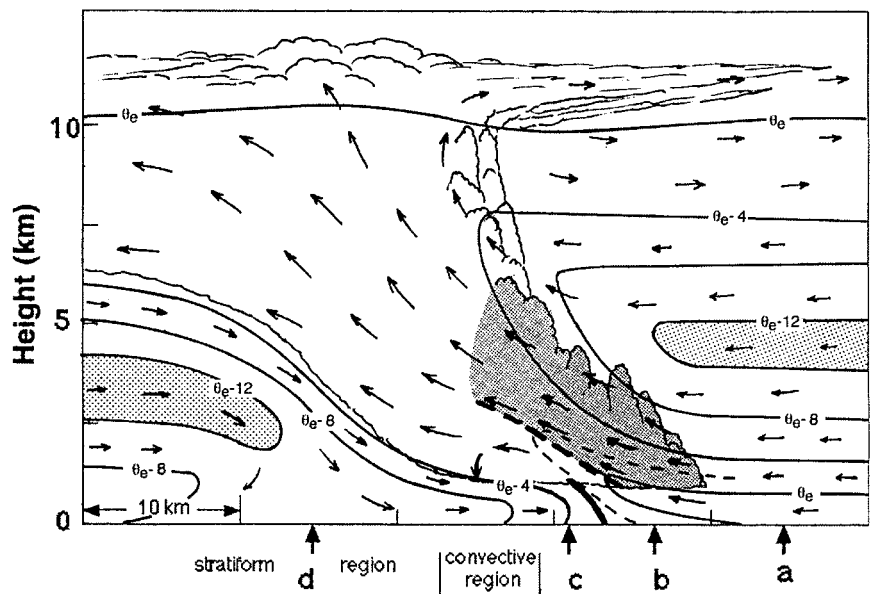


FIG. 5. Idealized cross section through slab convective overturning. Flow vectors are system-relative, scalloped lines indicate cloud boundaries, solid lines are  $\theta_e$  contours every 4 K (thin dashed line is an intermediate contour and heavy dashed line marks axis of highest values), heavy solid line indicates outflow boundary or frontal zone, light shading highlights midlevel layer of low  $\theta_e$  air, and dark shading depicts the MAUL. Points a–d indicate the locations of the soundings in Fig. 4.

lifted strongly such that a layer of the lower troposphere saturates, thereby creating a MAUL.

Conventional theory states that a MAUL will be quickly removed by nonhydrostatic buoyancy-driven overturning, that is, convective clouds will quickly develop and replace the MAUL with a moist neutral (or stable) profile. However, this conventional view based only on parcel theory does not account for the deep layer of powerful mesoscale vertical motion that created the MAUL in the first place. It is likely that the buoyancy-driven vertical motion that can remove the MAUL is actually less than the mesoscale vertical motion that created the MAUL. For example, consider first the vertical motions that parcel theory yields. Assuming that the environment shown in Fig. 4b is unchanging with time, parcel theory yields a vertical velocity of approximately  $6 \text{ m s}^{-1}$  for undilute ascent from 900 to 800 mb. However, as noted by Lucas et al. (1994a,b) and others, this vertical velocity value is likely to be a considerable overestimate of the actual buoyancy-induced vertical motion since it does not include such factors as mixing/entrainment and water loading. In fact, applying the simple cloud model of Anthes (1977), which includes entrainment and water loading, to the sounding shown in Fig. 4b produces vertical velocities that are generally less than two-thirds of the velocities that result from applying parcel theory.

Consider now the mesoscale vertical motions that are likely to occur in a typical MAUL environment wherein a low-level jet intersects a convectively generated mesoscale outflow boundary. For a  $10 \text{ m s}^{-1}$  low-level jet and a 1-km deep cold pool advancing at  $10 \text{ m s}^{-1}$ , the ascent would be  $2.0 \text{ m s}^{-1}$  if the lifting is distributed uniformly over a horizontal distance of 10 km. Of course, in many instances cold pools are deeper, low-level jets are stronger, and the lifting occurs over shorter distances so that the mesoscale ascent can be much stronger, that is, on the order of  $5\text{--}10 \text{ m s}^{-1}$ . Observations (e.g., Fig. 2) show that such large magnitudes of ascent can occur along mesoscale outflow boundaries—the zone where MAULs have been observed.

Thus, it appears possible that *there may be low-level layers in which the magnitude of dynamically driven mesoscale ascent can become comparable to or even exceed the magnitude of nonhydrostatic parcel vertical motions forced by buoyancy*, thereby facilitating the formation and maintenance of a MAUL. Moreover, if the changes in the mesoscale environment as a result of the strong mesoscale ascent are considered, the likelihood that the mesoscale ascent

will be larger than the buoyancy-forced vertical motions is even greater. This is because lifting a moist absolutely unstable layer *warms* the environment. Therefore, the temperature difference between a parcel and its environment would tend to be less when a MAUL is present than when the atmosphere is relatively quiescent.

To illustrate the differences in parcel ascent in quiescent and strongly ascending environments, consider a mesoscale area with a sounding (Fig. 6a) that exhibits a MAUL similar to that shown in Fig. 4b. If parcel theory is assumed, a parcel rising from the 1.0-km level will arrive at the 3.5-km level in 431 s with a vertical velocity of  $15.3 \text{ m s}^{-1}$ . When the parcel arrives at this level, it will be  $2.5^\circ\text{C}$  warmer than the environment. Even after considering entrainment and water loading (which would reduce the vertical velocity of the parcel by about 1/3), it is clear that the parcel would still quickly accelerate upward and would be considerably warmer than the environment.

Consider now what happens if there is strong mesoscale dynamically driven ascent ( $\bar{w}$ ). Assume that  $\bar{w}$  is  $5 \text{ m s}^{-1}$  at the 1.0-km level and that it increases with height in the lower troposphere according to

$$\frac{\partial \bar{w}}{\partial z} = 1 \text{ m s}^{-1} \text{ km}^{-1}.$$

Assume also that horizontal advection can be ignored and that, due to some local effect, a parcel embedded within the mesoscale environment arrives at the 1.0-km level with a vertical motion of  $5.5 \text{ m s}^{-1}$  ( $0.5 \text{ m s}^{-1}$  faster than the mesoscale environment). After about 400 s (Fig. 6b), the environment will change (warm) to that shown in Fig. 6c. The parcel rising from the 1.0-km level will arrive at the 3.5-km level with a vertical velocity of  $7.7 \text{ m s}^{-1}$  and will be  $0.5^\circ\text{C}$  warmer than its environment (Fig. 6d). Note that, even though the parcel in this ascending environment started with a large vertical velocity ( $5.5 \text{ m s}^{-1}$ , as opposed to  $0 \text{ m s}^{-1}$  for the quiescent environment case), it arrives at the 3.5-km level with a vertical velocity considerably less than the quiescent case ( $7.7 \text{ m s}^{-1}$  as opposed to  $15.3 \text{ m s}^{-1}$ ), and that it is only  $0.5^\circ\text{C}$  warmer than the environment (as opposed to  $2.5^\circ\text{C}$  for the quiescent case). Furthermore, since  $\bar{w}$  at 3.5 km is  $7.5 \text{ m s}^{-1}$ , the parcel in the ascending environment case is rising only  $0.2 \text{ m s}^{-1}$  faster than its environment, while the parcel in the quiescent environment is rising  $15.3 \text{ m s}^{-1}$  faster than its environment.

This example shows how strong mesoscale ascent of a MAUL would tend to reduce the temperature *difference* between a parcel and its environment to values smaller than that which would be expected if the environment were quiescent, thereby decreasing the buoyancy-driven acceleration of the parcel. This is because of the important, but often overlooked, aspect of moist absolutely unstable layers—that ascent in these conditions produces local warming (cf. the 2–4-km layer in Figs. 6a and 6c). This effect favors the perpetuation of the MAUL until parcels reach the middle troposphere where temperature differences between buoyancy-driven parcels and the mesoscale environment may finally become large enough for individual buoyant updrafts to emerge.

This proposed conceptual model for the formation and maintenance of moist absolutely unstable layers is, in some respects, analogous to the manner in which dry absolutely unstable layers are created and sustained in that it evolves as a result of a *rate imbalance*. In the dry case, the imbalance arises because the heating of air in the surface layer exceeds the rate at which dry convective eddies can carry the heat upward. In this situation, the vertical temperature gradient increases, even to the point where it exceeds the dry-adiabatic lapse rate. In the moist case, the agent for creating the absolutely unstable layer is not radiative heating at the surface—rather, it is the dynamically driven environmental vertical motion,  $\bar{w}$ . Specifically, if

$$\bar{w} \geq w',$$

where  $w'$  represents the buoyancy-driven vertical motion of a parcel, then the rate at which mesoscale ascent creates the moist absolutely unstable condition will be greater than the rate at which cloud-scale turbulent eddies can overturn and eliminate the absolutely unstable layer. For example, if an entire low-level layer of the environment were ascending at  $10 \text{ m s}^{-1}$  but the strongest vertical motions that buoyancy forces could create in that layer were only  $5 \text{ m s}^{-1}$ , then there could

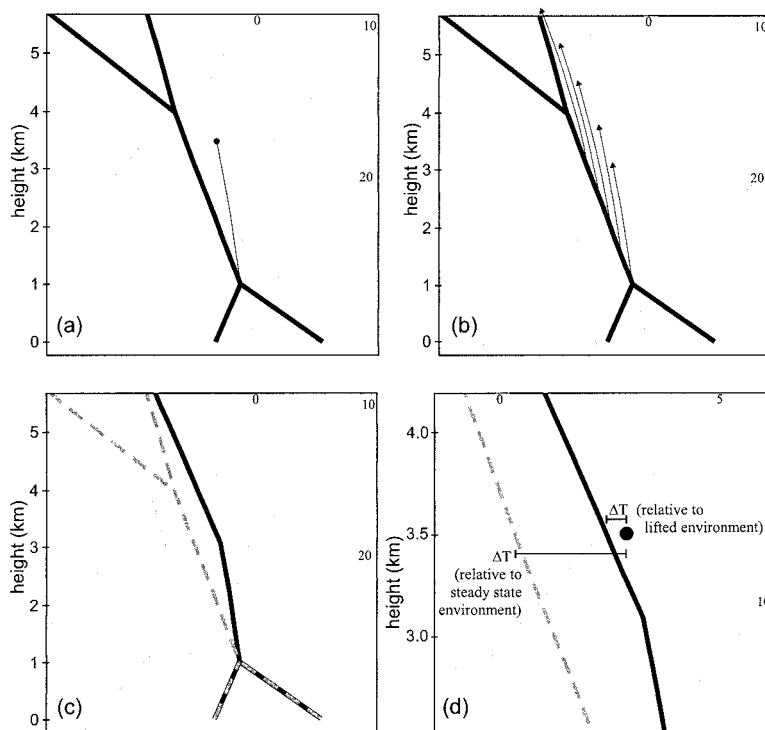


FIG. 6. A comparison of the buoyancy of a parcel ascending in a static moist absolutely unstable environment vs a parcel ascending in a rapidly rising moist absolutely unstable environment. (a) Parcel path ascending within a steady-state environment. Thick solid lines depict the steady-state environmental sounding; thin solid line represents a path of undilute moist-adiabatic ascent for a parcel starting at 1 km above ground. The dot is the location of the parcel after 431 s. (b) Illustration of the change in environmental profile as a result of strong lower tropospheric mesoscale ascent. Arrows indicate the path of the ascending layer. (c) The new environmental sounding after 400 s of lifting (thick solid black lines). Gray dashed lines are the initial environmental sounding shown in (a). (d) Temperature differences ( $\Delta T$ ) between a parcel (black dot) and the ascending environment (solid black line) and  $\Delta T$  between the parcel and a steady-state environment (dashed gray line). Note that the dot in (d) is at the same temperature and elevation as in (a). In all panels, solid gray lines are isotherms and thin dashed gray lines are moist adiabats.

be no buoyancy-driven descending air. The atmosphere would continue to ascend everywhere in the layer and therefore the moist absolutely unstable condition would persist.

Note that  $w'$  is proportional to the vertical integral of the temperature difference between the parcel and the environment, that is, it is proportional to convective available potential energy (CAPE). Thus, the *vertical distribution of CAPE in the low levels*, not just the total value of CAPE for the entire sounding, may be important in determining the organizational mode in the convective region of MCSs, that is, whether the convective region appears solid or cellular. A large value of low-level CAPE (implying a large value of

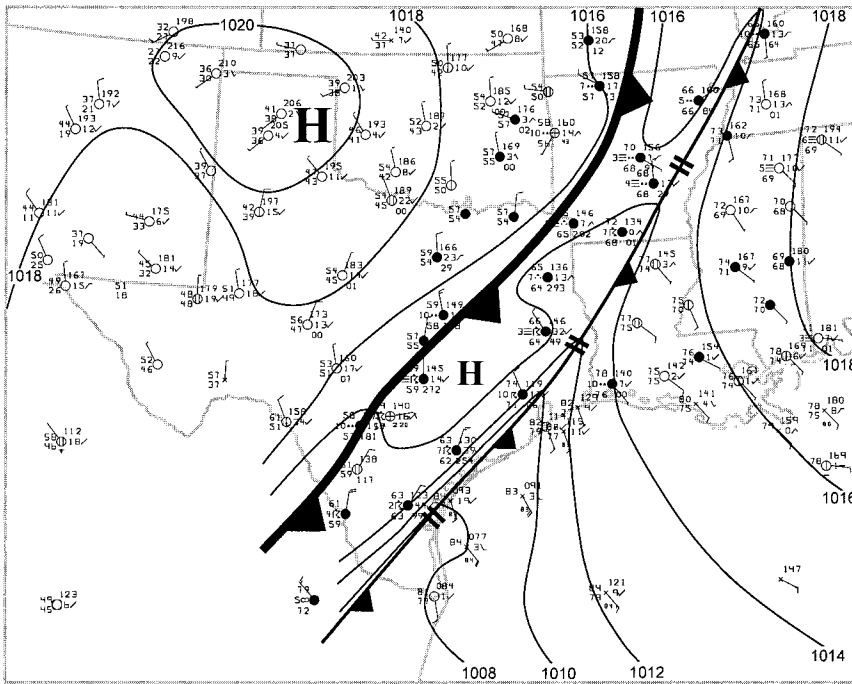


FIG. 7. Subjective surface mesoanalysis at 1200 UTC 6 Oct 1998. Contour interval is 2 mb. Analysis convention follows Young and Fritsch (1989).

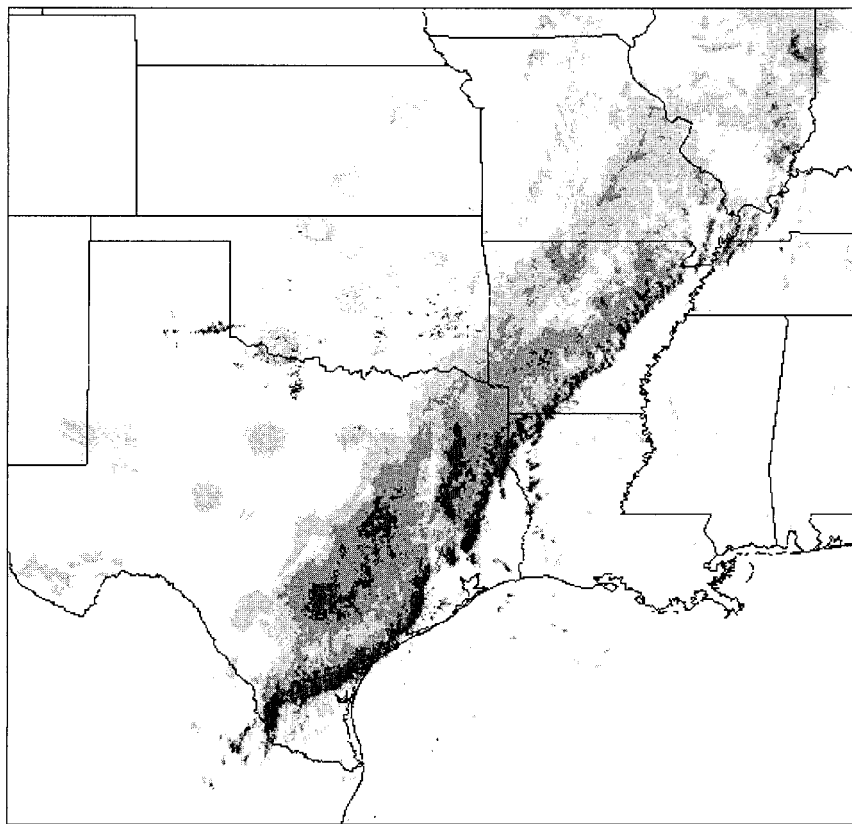


FIG. 8. Regional radar composite at 1200 UTC 6 Oct 1998. Four levels of shading correspond to, from lightest to darkest, 15–30, 30–40, 40–50, and > 50 dBZ.

$w'$  at low levels) increases the likelihood that isolated parcels will develop vertical motions larger than the environmental ascent, and therefore cellular updrafts will dominate rather than the slab ascent.

#### 4. Numerical simulation

To address the issues raised by the observations and our conceptual model of moist absolute instability, a mesoscale convective system was simulated with a very high-resolution numerical model. An event that featured a developing MAUL in the standard sounding network was selected.

##### a. Description of the event

The convective system initiated along a cold front over the southern Great Plains on the evening of 5 October 1998. During the overnight hours, the convective system advanced several hundred kilometers ahead of the cold front and by 1200 UTC displayed a nearly continuous convective line and trailing stratiform region from southern Texas to northeastern Arkansas (Figs. 7 and 8). The surface inflow was nearly perpendicular to the convective line indicating that strong lower-tropospheric ascent was occurring along the mesoscale outflow boundary. Upper-air analyses (e.g., Fig. 9) reveal that the inflow to the convective system extended through a deep layer and was very moist (dewpoint depressions along the convective line were generally  $\leq 5^\circ\text{C}$ ).

Of particular interest to this study is the sounding from Corpus Christi, Texas (CRP)

(Fig. 10a). This sounding contains three MAULs separated by pockets of moist but unsaturated air. The first MAUL above the surface is 100 mb deep, and has a lapse rate significantly greater than the moist-adiabatic lapse rate. NEXRAD data (Fig. 11), taken at the same time that the sounding was released, reveal an approaching outflow boundary only 25 km away from the rawinsonde facility (which is collocated with the NEXRAD facility). Assuming the CRP sounding was released on time (rawinsondes are supposed to be released at 1100 UTC), then it sampled the environment immediately ahead of the convective line where strong mesoscale lifting was likely to be occurring. The NEXRAD data display a nearly solid swath of reflectivity greater than 40 dBZ, which is further evidence of strong low-level mesoscale ascent and indicative of slab convective overturning.

The data from the CRP sounding compares favorably with the nearby sounding at Brownsville, Texas (BRO), which was released well ahead of the convective line (Fig. 10b). Specifically, if about 50 mb of low-level lifting is applied to the BRO sounding, the result resembles the CRP sounding. Furthermore, when the CRP sounding is considered within the context of constant pressure plots (Fig. 9), it matches the synoptic analyses of temperature, height, and wind. This suggests that the CRP sounding actually represents the inflow environment to the convective system, and that it was not “contaminated” by one of the processes listed in section 2 that could create incorrect MAUL-like structures in rawinsonde ascents.

### b. Model description and experimental design

A multiple-nested version of the Pennsylvania State University–National Center for Atmospheric Research Mesoscale Model (MM5; Dudhia 1993) was used for the numerical simulation. The experiment was designed such that the innermost domains could explicitly resolve convective processes using the model’s nonhydrostatic equations. Recent studies have demonstrated the ability of MM5 to

explicitly reproduce convective processes and mesoscale convective systems [e.g., Liu et al. (1997), a simulation of Hurricane Andrew; and Skamarock (1994), simulations of supercell thunderstorms].

The experimental design is summarized in Table 3, and the model domains are illustrated in Fig. 12. The two coarse-resolution domains (domain 1,  $\Delta x = 36$  km; and domain 2,  $\Delta x = 12$  km) were initialized with gridded fields from the National Centers for Environmental Prediction (NCEP). The NCEP fields were also used as boundary conditions for domain 1. Domains 1 and 2 were two-way interactive such that the boundary conditions for domain 2 were supplied by domain 1 at every time step. The explicit moisture scheme of Reisner et al. (1998) was used in conjunction with the Kain and Fritsch (1990) convective parameterization. The Reisner scheme contains predictive equations for cloud water, rain, snow, ice, and graupel.

Domain 3 used a grid spacing of 4 km. Output from domain 2 (including cloud and precipitation fields) served as initial conditions and boundary conditions for domain 3. Following the work of Weisman et al. (1997), no convective parameterization was applied. Thus, the nonhydrostatic model equations produce all convective overturning. The subgrid-scale turbulence

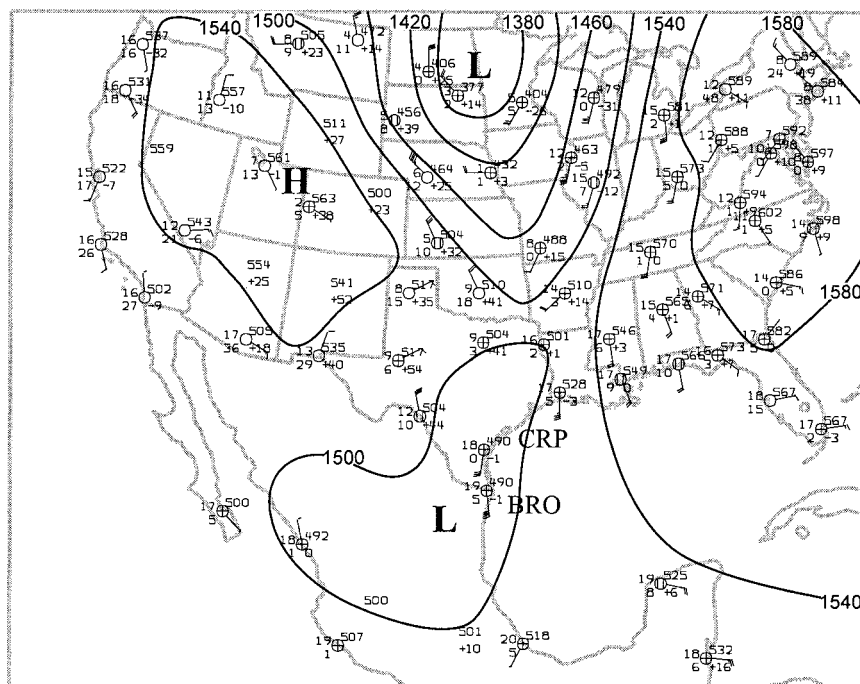


FIG. 9. Subjective analysis of 850-mb geopotential height (contour interval 40 m) at 1200 UTC 6 Oct 1998. The locations of Corpus Christi, TX (CRP), and Brownsville, TX (BRO), are indicated.

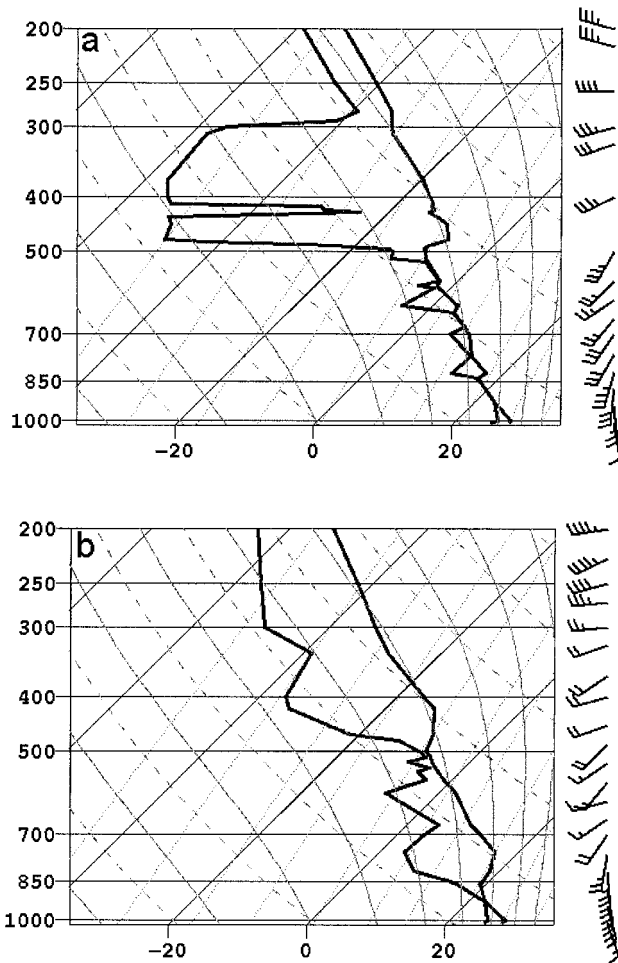


FIG. 10. Observed soundings at 1200 UTC 6 Oct 1998: (a) CRP, (b) BRO.

parameterization is based on K theory and accounts for fluxes of momentum, potential temperature, mixing ratio, and microphysical quantities. The eddy coefficients (K values) are based on the local Richardson number, which has a different formulation for saturated and unsaturated conditions, and on the local momentum deformation.

The output from domain 3 provided the initial and boundary conditions for a very high-resolution run (domain 4,  $\Delta x = 1.33$  km). No convective parameterization was used on this domain, and the subgrid-scale turbulence scheme is the same as that used on domain 3. The following section presents analyses from domains 3 and 4 to examine the properties of MAULs.

### c. Analysis of the spatial and temporal scale of moist absolute instability

In general, the simulation of the surface features (not shown) compares favorably with the surface me-

soanalysis and with the radar reflectivity pattern (cf. Figs. 8 and 13). Most importantly, both experiments with nonhydrostatic explicit convection (i.e., domains 3 and 4) generate MAULs. Sample soundings from the southwestern portion of domain 4 are included as an example (Fig. 14). These soundings reveal the transition from an initially unsaturated environment ahead of the convective system (Fig. 14a) to a state that resembles the CRP sounding just ahead of the outflow boundary (cf. Figs. 10a and 14b). Above the outflow boundary, there is a 300-mb deep MAUL (Fig. 14c). Farther back into the system, that is, in the stratiform region, the profile is approximately moist neutral in the middle and upper troposphere with a weak “onion” (Zipser 1977) structure at low levels (Fig. 14d).

Figure 15 displays the horizontal distribution of the saturated<sup>4</sup> unstable layer. A MAUL at least 100 mb deep stretches continuously along and rearward of a zone of strong ( $> 1 \text{ m s}^{-1}$ ) low-level mesoscale ascent (Fig. 16) where the outflow boundary of moist-downdraft-generated cold air forces warm moist air upward. The magnitude of the upward motion is consistent with the earlier estimates of vertical motions forced by low-level inflow overriding advancing cold pools (section 2b) and with Doppler-radar-observed values (cf. Figs. 2 and 16). Figure 15 confirms one reason why MAULs are difficult to capture with rawinsonde ascents, that is, the MAUL layer is only a few kilometers to a few tens of kilometers wide. Thus, a balloon must be released only a few minutes before the outflow boundary passes in order to sample the MAUL.

Examination of the conditions during passage of the convective system reveals that the moist absolutely unstable state typically lasted about 30 min at most individual grid points (e.g., Fig. 17a) but persisted for up to 45 min at some points. Thus, the model simulation supports the contention that MAULs can last for time periods longer than the lifetime of individual moist convective elements. Also, note that the MAUL is created where powerful low-level upward motion lifts the conditionally unstable environment to saturation (Fig. 17b). After the strongest ascent ceases (after 1100 UTC in Fig. 17), the MAUL begins to weaken in intensity and depth, presumably due to turbulent mixing. It is not until after all positive vertical motion ceases that the MAUL disappears.

<sup>4</sup>A grid point in the model is considered saturated if the cloud water mixing ratio exceeds  $0.01 \text{ g kg}^{-1}$ .

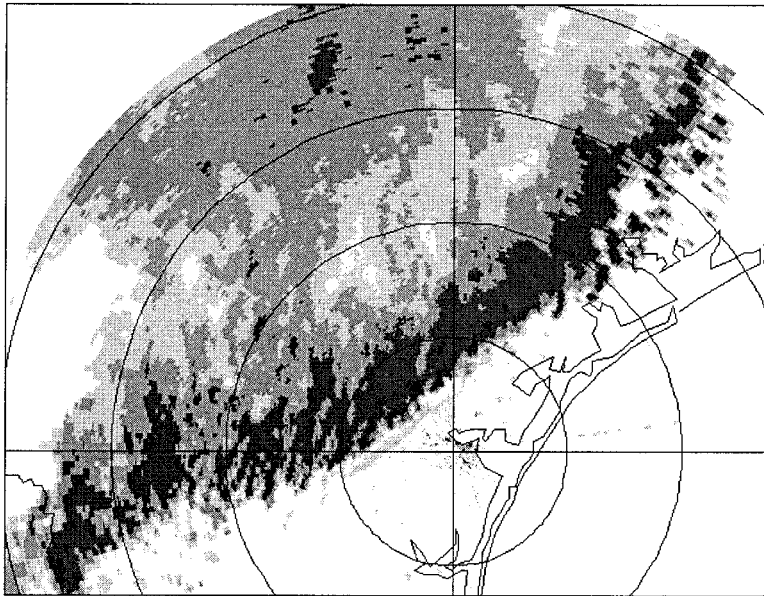


FIG. 11. WSR-88D base reflectivity image (0.5° elevation) from CRP at 1056 UTC 6 Oct 1998. Shading is the same as in Fig. 8.

Parcel trajectories were computed from 1-min-resolution model output. Analysis of conditions along the trajectories shows that moist absolutely unstable conditions are experienced by parcels for 15 min or more. Note that this result from a Lagrangian reference frame agrees with the result from the Eulerian reference in the previous paragraph, since the mean movement of the MCS is southeast at  $12 \text{ m s}^{-1}$  and the mean wind speed in the MAUL is  $15 \text{ m s}^{-1}$ . Using these values, and assuming a mean MAUL width of 20 km, moist absolutely unstable conditions would be expected to last for 28 min in an Eulerian reference frame and for 12 min in a Lagrangian reference frame.

It is interesting that deep convective overturning never occurs at the grid point in Fig. 17, despite the existence of a deep, long-lived, absolutely unstable layer. Conventional parcel theory states that buoyancy-driven cumulonimbus convection would ensue under these conditions. Deep penetrative thunderstorm cells do, however, develop in other portions of the MAUL. These cells are evident on constant- $\sigma$ -level analyses (e.g., Fig. 18c) and on vertical cross sections (Fig. 19a) as towers of locally warm  $\theta_e$

anomalies that emerge at middle and upper levels. The towers of high  $\theta_e$  air are surrounded on all sides by much lower (by several K)  $\theta_e$  values and fit the traditional view of thunderstorm “cells” (Byers and Braham 1948) and “hot towers” (Riehl and Malkus 1958). In contrast to the localized “bubbles” at upper levels, the distribution of  $\theta_e$  in the MAUL has a considerably different structure. The highest  $\theta_e$  air in the MAUL extends in a contiguous swath across the domain (Fig. 18b). Note, also, that the highest  $\theta_e$  air from the boundary layer “disappears” as it is mixed in the MAUL (Figs. 17c and 19a). Only a small percent of the broad swath of high  $\theta_e$  boundary layer (Fig. 18a) actually reaches higher levels with little mixing (Fig. 18c).

#### d. Analysis of buoyancy

The existence of cellular  $\theta_e$  towers emanating from some locations within a MAUL raises the question of how buoyancy works in MCSs. The magnitude of

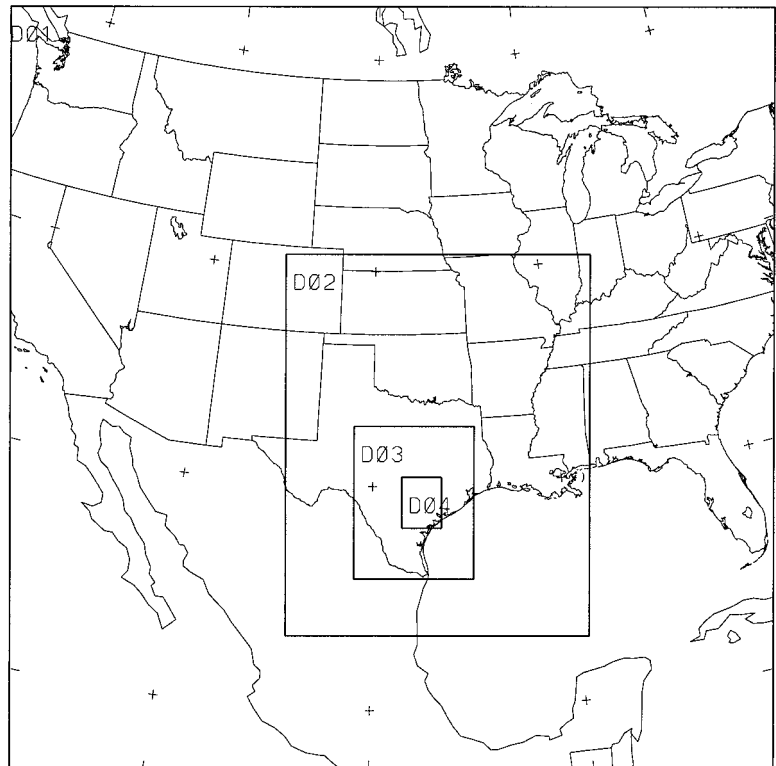


FIG. 12. Configuration of model domains.

TABLE 3. Design of numerical simulation

Domain ID:	1	2	3	4
Horizontal grid spacing, dx (km)	36	12	4	1.33
Grid points (north–south) × (east–west)	109 × 109	163 × 130	196 × 154	196 × 154
Vertical layers	39	39	39	39
Explicit precipitation	Reisner et al. (1998)	Reisner et al. (1998)	Reisner et al. (1998)	Reisner et al. (1998)
Convective parameterization	Kain and Fritsch (1990)	Kain and Fritsch (1990)	None	None
Initial conditions	NCEP	NCEP	Domain 2	Domain 3
Boundary conditions	NCEP	Domain 1	Domain 2	Domain 3
Initialization time	0000 UTC 6 Oct	0000 UTC 6 Oct	0600 UTC 6 Oct	0900 UTC 6 Oct
Forecast length	24 h	24 h	9 h	3 h

buoyancy is typically defined as being proportional to the difference between the local virtual temperature<sup>5</sup> ( $T'_v$ ) and the environmental virtual temperature ( $\bar{T}_v$ ). From parcel theory, the vertical acceleration of a parcel due to buoyancy is

$$\frac{\partial w}{\partial t} = g \frac{T'_v - \bar{T}_v}{\bar{T}_v}. \quad (1)$$

Although parcel theory concepts are routinely applied, a consistent definition for  $\bar{T}_v$  does not exist. The cellular towers in Figs. 18c and 19a are surrounded on all sides by colder environmental air. Thus, one might define  $\bar{T}_v$  as the temperature some small distance away from (but not inside) one of these towers. This definition is consistent with observational studies of cumulus clouds, where buoyancy is typically defined as the temperature measured inside the cloud minus the temperature just outside of the cloud. In contrast, it is more difficult to define the buoyancy of a parcel

within the saturated high  $\theta_c$  swath of Fig. 18b. Temperatures in the direction perpendicular to the axis of the high  $\theta_c$  swath are cooler, whereas neighboring parcels within the swath have nearly identical temperature. Therefore, it is unclear how to define  $\bar{T}_v$  for a parcel in the high  $\theta_c$  swath. Perhaps  $\bar{T}_v$  should be defined as the average temperature around a circle centered on a parcel, rather than the temperature in one randomly chosen direction.

The different environments of parcels in a slab versus parcels in cellular towers are further illustrated in Figs. 20 and 21. A  $\theta_c$  cross section taken *perpendicular* to the outflow boundary is presented in Fig. 20. Three  $\theta_c$  cross sections taken *parallel* to the outflow boundary are presented in Fig. 21: one is in the conditionally unstable environment ahead of the MCS (Fig. 21a), one is just behind the surface outflow boundary (Fig. 21b), and one is through a convective tower trailing behind the outflow boundary (Fig. 21c). Notice in these cross sections how the horizontal gradient of  $\theta_c$  varies as the layer of high  $\theta_c$  air ascends in the slab. The value of buoyancy at points A, B, and C in these cross sections would produce large differences depending on how  $\bar{T}_v$  is defined. Specifically, Table 4 lists the virtual temperature difference ( $\Delta T_v = T'_v - \bar{T}_v$ ) between each grid point and the virtual tem-

<sup>5</sup>Virtual potential temperature is also widely used in definitions of buoyancy.

perature 3 km<sup>6</sup> away from the grid point in various directions. As noted above, there are points within the unstable slab (e.g., point B) where, for all practical purposes, the temperature is the same as neighboring points within the slab (as noted by  $\Delta T_e$  and  $\Delta T_w$  in Table 4). Only the temperature difference in the north and south direction would produce large positive buoyancy. In contrast, point C is surrounded on all sides by colder air and should be experiencing the strongest buoyancy-induced vertical acceleration by Eq. (1).

Thus, it seems that buoyancy acting on parcels in the low-level swath of high  $\theta_e$  air (i.e., in the MAUL) would tend to be smaller than buoyancy acting on parcels within towers emerging from the MAUL. Moreover, as discussed in section 3b, because the low-level environment is rising moist adiabatically nearly as fast as the parcels, the temperature difference between parcels and the environment remains much smaller than that expected from traditional applications of parcel theory. In summary, buoyancy-induced accelerations in the MAUL are likely to be much smaller than that suggested by parcel theory, which further supports the notion that small-scale moist convection will not remove a saturated absolutely unstable state as quickly as conventional wisdom expects.

*e. Analysis of the mean state*

Another intriguing characteristic revealed by cross sections through the convective line is the development of the moist stable mean state well behind the outflow boundary, that is, in the stratiform region. Individual cross sections through the system (e.g., Fig. 19) always contain complicated and potentially confusing structures. Yet overall, it is clear that the conditionally unstable state in the prestorm environment (the far right side of Fig. 19a) is eventually transformed to a stable (relative to moist vertical mixing) environment (the left side of Fig. 19a).

<sup>6</sup>There is no physical significance to choosing 3 km here. The qualitative results of this experiment will not change if a smaller or larger (by 1–5 km) distance is chosen.

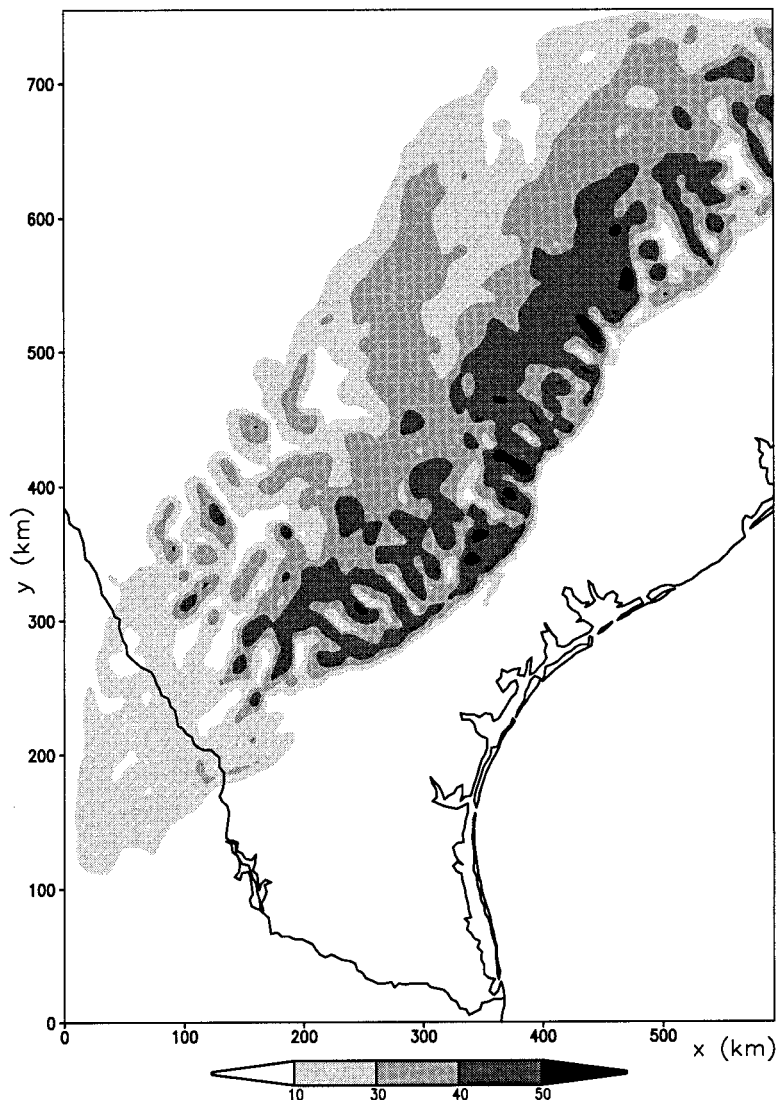


FIG. 13. Simulated reflectivity (dBZ) from domain 3 at 1115 UTC 6 Oct 1998.

To obtain an appreciation for the mean state of the convective system rather than individual snapshots through convective elements, horizontal and temporal averaging was performed to obtain a cross-section

TABLE 4. Difference in virtual temperature (°C) between the grid points in Figs. 20–21 and points 3 km to the east ( $\Delta T_e$ ), west ( $\Delta T_w$ ), north ( $\Delta T_n$ ), and south ( $\Delta T_s$ ).

	$\Delta T_e$	$\Delta T_w$	$\Delta T_n$	$\Delta T_s$	Average
A	-0.04	0.04	-0.02	0.02	0.00
B	-0.02	-0.01	+2.67	+1.18	+0.96
C	+2.68	+2.10	+2.00	+1.93	+2.18

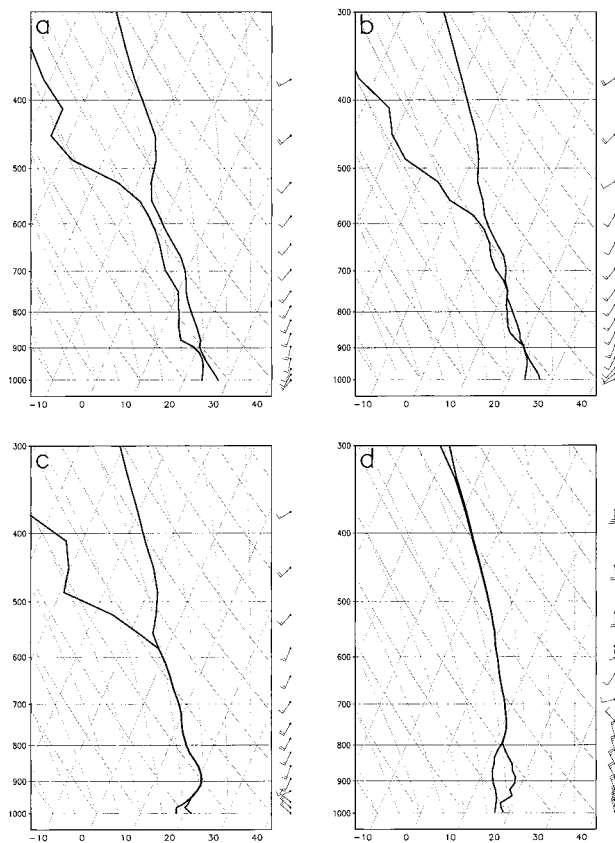


FIG. 14. Soundings from domain 4 at 1100 UTC 6 Oct 1998.

averaged state. The temporal averaging was performed using model output at 1-min increments over a 30-min period. The resulting mean fields reveal that the MAUL weakens rearward of the leading edge, thereby creating the stable (relative to moist mixing) profile (Fig. 22a). In the absolutely unstable slab, high  $\theta_e$  air from the base of the MAUL is mixed with low  $\theta_e$  air from the top of the MAUL. Since parcels in a MAUL are unstable if displaced up or down (as long as they remain saturated), this mixing process is very efficient. High-resolution three-dimensional time animations show that this vertical mixing is accomplished primarily by saturated eddies that bring “blobs” of midlevel low  $\theta_e$  air downward while simultaneously carrying high  $\theta_e$  boundary layer air upward. Moreover, Droegemeier and Wilhelmson (1987) showed that the strongly sheared interface region between the ascending slab and the colder air below is highly turbulent. Therefore, the top and bottom of the MAUL layer would be expected to exhibit strong moist mixing. The small-scale overturning would entrain mass into the top and bottom of the slab. This conceptual model suggests that some mesoscale convective systems

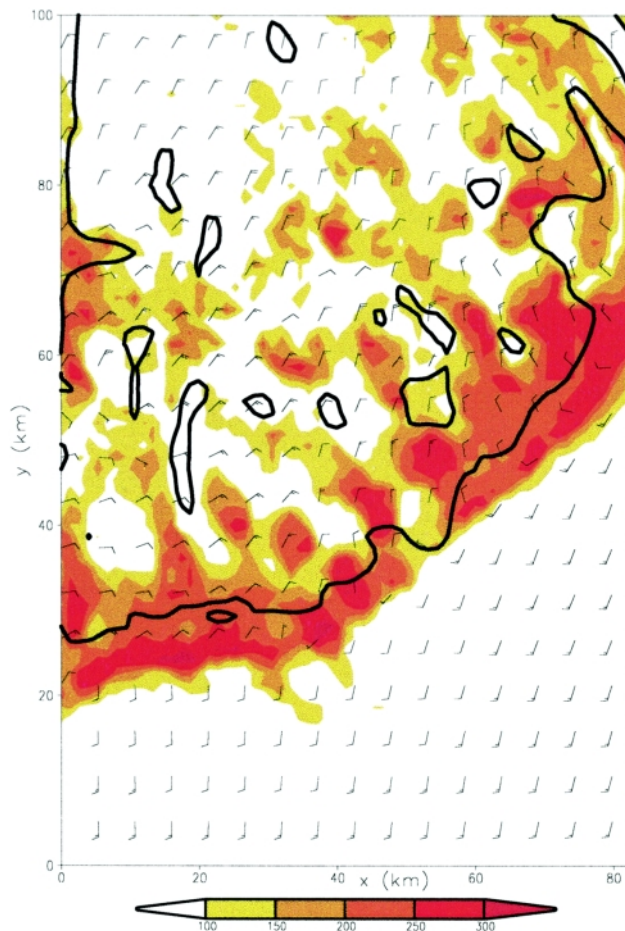


FIG. 15. Graphical depiction of regions where a moist absolutely unstable layer exists (shading), simulated reflectivity  $\geq 30$  dBZ (bold contour) at  $\sigma = 0.780$  (about 800 mb), and surface wind barbs from domain 4 at 1100 UTC 6 Oct 1998. Levels of shading represent the depth (mb) of the moist absolutely unstable layer.

could be characterized as *vertically expanding slabs of saturated buoyantly turbulent flow composed of a continuous spectrum of moist buoyant elements*. The mean cross section also reveals that, despite the existence of locally downward-moving air, the mean vertical velocity in the MAUL is upward everywhere (Fig. 22b). Doppler radar studies of the mean vertical velocity in both convective and stratiform regions of MCSs have produced the same conclusion (e.g., Gamache and Houze 1982; Srivastava et al. 1986).

## 5. Implications to the conceptual model of mesoscale convective systems

The observations and model output of moist absolutely unstable conditions supports a conceptual model

of MCSs as vertically expanding slabs of moist, turbulent mixing. This conceptual model agrees with the interpretation of other investigators (e.g., Yuter and Houze 1995) who demonstrated that a full spectrum of convective overturning accomplishes the vertical mass transport in MCSs; that is, the transport is not dominated by a few large convective towers with intervening subsaturated areas.

The results also suggest that the differentiation between “convective” and “stratiform” regions of some MCSs is not always distinct. Rather, continuous moist turbulent mixing can extend from the conditionally unstable inflow environment at the front of the system to the moist neutral state at the rear of the system. This interpretation agrees with other studies [e.g., Zipser et al. (1983) and Leary and Rappaport (1987), both based on radar analyses], who noted that the region between the convective and stratiform regions was not an abrupt transition from convective towers to stratiform precipitation; rather, the transition was accomplished gradually, though not uniformly, with

a decreasing number of convective towers farther back into the convective system.

If the formation of a MAUL does coincide with strong but predominantly small-scale moist mixing, it would help to explain two features often observed with mesoscale convective systems:

- the highest values of equivalent potential temperature ( $\theta_e$ ) evident in the inflow to the mesoscale slab of ascent disappear as the flow passes upward through the MAUL (e.g., Zipser et al. 1981; Rotunno et al. 1988); and
- the culmination of this mixing process is the transformation of the MAUL into a deep, saturated, nearly uniform value of  $\theta_e$  (i.e., moist neutral state) over a *mesoscale region* in the upper half of the troposphere.

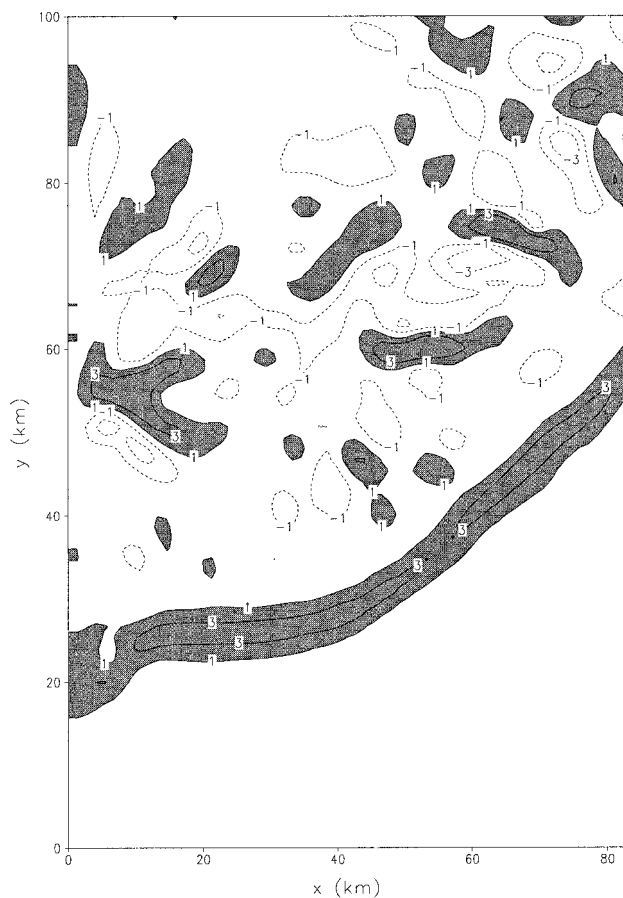


FIG. 16. Vertical velocity ( $\text{m s}^{-1}$ ) at  $\sigma=0.900$  (about 1 km above ground) from domain 4 at 1100 UTC 6 Oct 1998.

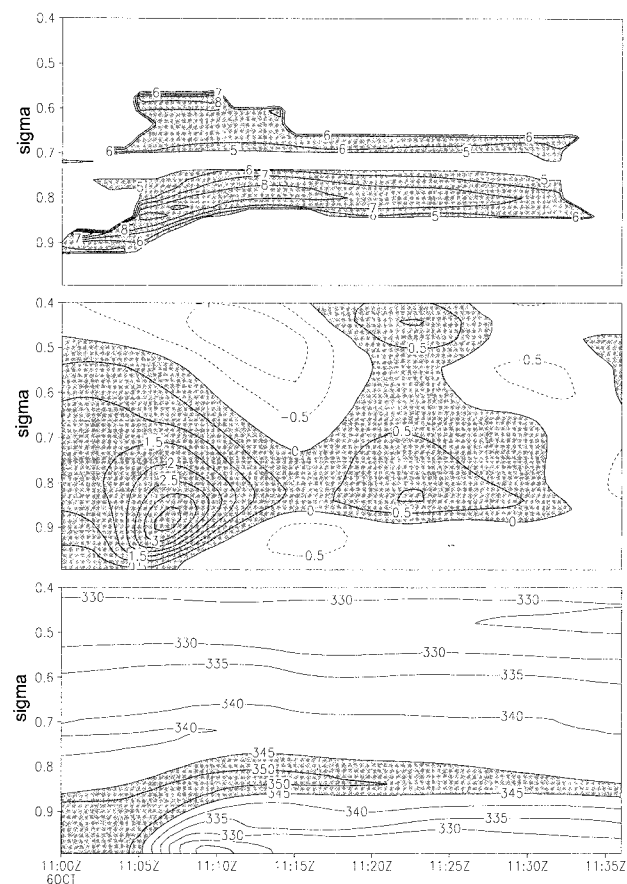


FIG. 17. Time series of conditions at a grid point from domain 4. (top) Depiction of times when a MAUL existed at the grid point (shading). Contours represent the lapse rate of temperature within the MAUL (in  $\text{K km}^{-1}$ ). (middle) Vertical velocity ( $\text{m s}^{-1}$ , contour interval  $0.5 \text{ m s}^{-1}$ , values  $> 0$  are shaded). (bottom)  $\theta_e$  (K, contour interval 5 K, values  $> 345 \text{ K}$  are shaded). Time resolution is 1 min. The grid point in this analysis is the same as that presented in Fig. 14b.

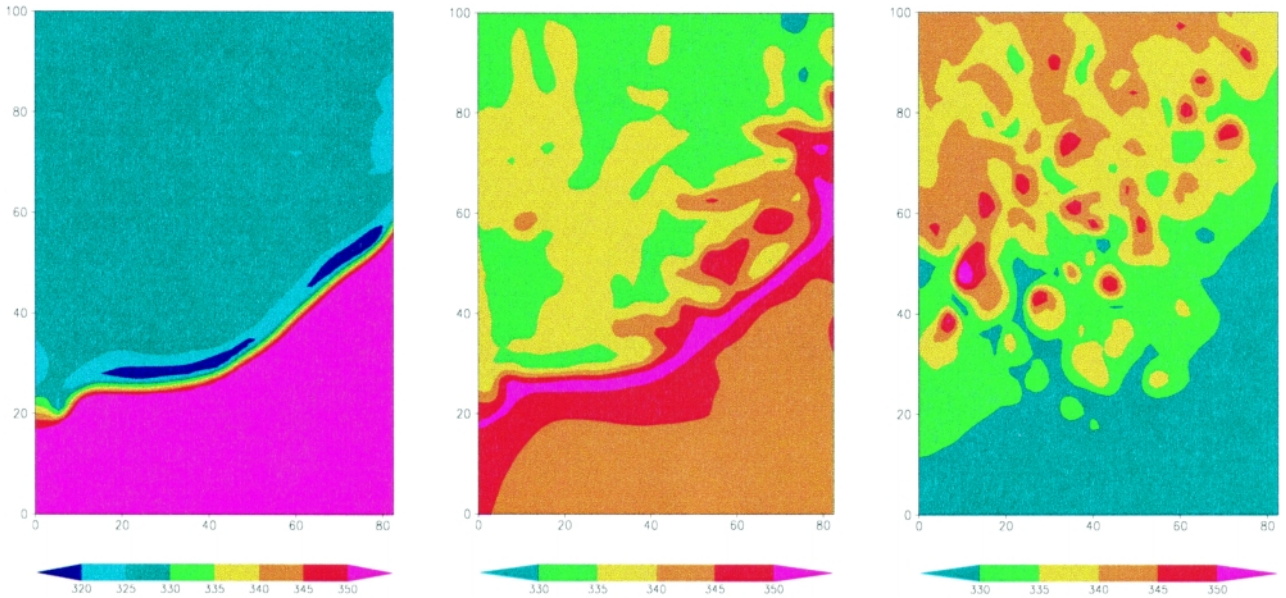


FIG. 18. Equivalent potential temperature ( $\theta_e$ ) from domain 4 at 1100 UTC 6 Oct 1998: (left)  $\sigma = 0.995$  (lowest model level), (center)  $\sigma = 0.860$  (about 850 mb), and (right)  $\sigma = 0.480$  (about 500 mb). Shading interval is 5 K.

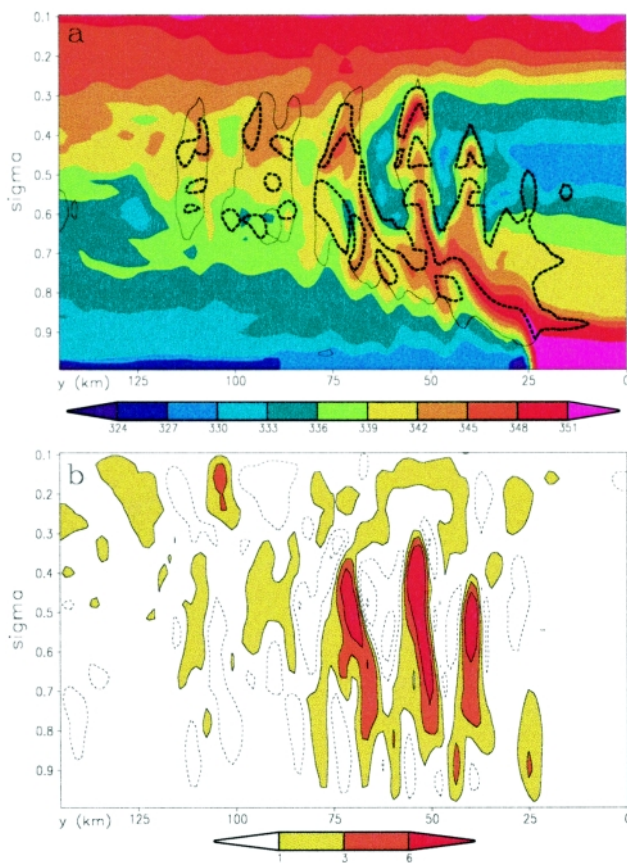


FIG. 19. Cross sections from domain 4 at 1100 UTC 6 Oct 1998: (a) equivalent potential temperature (shaded, K) and cloud water (contour, representing  $1 \text{ g kg}^{-1}$ ), (b) vertical velocity, where dashed contours correspond to  $-6$ ,  $-3$ , and  $-1 \text{ m s}^{-1}$ , and solid contours correspond to  $+1$ ,  $+3$ , and  $+6 \text{ m s}^{-1}$ .

The second feature, a nearly uniform value of  $\theta_e$ , is most readily evident in the upper portion of “onion” soundings taken through the trailing stratiform regions of MCSs (e.g., Fig. 4d; Zipser 1977; Leary 1980). Note that this view simplifies the problem of how deep convection transforms its initially subsaturated, stably stratified, midlevel environment into the *mesoscale region* of saturated near-neutral condition observed in the trailing stratiform region. It seems difficult, if not impossible, to create this latter condition with a collection of cumulonimbus towers. Also note that mesoscale regions of saturation obtained through slab overturning facilitates arguments for production of dynamically balanced mesoscale structures by moist convection, since it eliminates the problem of having to explain away gravity wave energy losses and the lack of midlevel detrainment from deep convective towers.

The existence of slab convective overturning highlights two fundamental problems with convective parameterization in mesoscale models: 1) that buoyant parcels sometimes follow slantwise paths and traverse more than a single grid element in a convective cloud life cycle, and; 2) that even if saturation occurs in a conditionally unstable environment, there is no guarantee that deep moist convective towers will develop. Therefore, the simple cloud models used in convective parameterization cannot accurately represent the convective processes that occur in MCSs. Nevertheless, Kain and Fritsch (1998) were able to show that, to a good approximation, the *combination* of parameter-

ized convection and resolvable-scale processes permits the formation of moist absolutely unstable layers and slantwise mesoscale ascent. When they forced the convective parameterization to eliminate the moist absolutely unstable layers as quickly as they formed, the solution became unphysical suggesting that the moist absolutely unstable layers play an important role in the overall convective process.

The occurrence of moist absolutely unstable layers may help explain why parcel vertical motions are sometimes much smaller than what would be expected from parcel theory (e.g., see LeMone and Zipser 1980; Zipser and LeMone 1980; Lucas et al. 1994a,b). A sounding through a moist absolutely unstable layer could show large CAPE, indicating that strong vertically upright upward motions should occur. However, as is evident in the Rotunno et al. (1988) simulation, the highest  $\theta_e$  air can rise in a slantwise manner while turbulent mixing simultaneously reduces the cloud-scale buoyancy. If this process is happening uniformly all along the slab, then the temperature of the environment on either side of an ascending parcel is essentially the same as the parcel's temperature. Since the environment of a parcel is colder only in two directions, one would expect the acceleration due to buoyancy to be less than that stated by parcel theory (where a lifted parcel is assumed to be surrounded by air of uniform properties). The exact consequences of this arrangement are, of course, unknown. Nevertheless, this conceptual model suggests that vertical accelerations should be much less than that based upon parcel theory.

It has been argued that moist symmetric instability can give rise to a slantwise-shaped updraft in mesoscale convective systems (e.g., Seman 1994). While this may be true for some mesoscale convective systems, the results here support slantwise updrafts without invoking (though not precluding) the existence of symmetric instability. For example, consider a stationary situation wherein a low-level jet overrides a surface-based outflow boundary and creates a saturated layer in a conditionally unstable environment. If the buoyancy-induced vertical motion is much smaller than the horizontal flow, the saturated parcels will be advected horizontally much faster than they will ascend, that is, slantwise flow results. Of course, in some instances, continued acceleration by buoyancy forcing eventually causes the vertical velocity to greatly exceed the horizontal velocity, thereby resulting in essentially upright flow and the emergence of convective towers. LeMone et al. (1984) presented a similar argument to explain the low tilt (about  $30^\circ$  above horizontal) of the

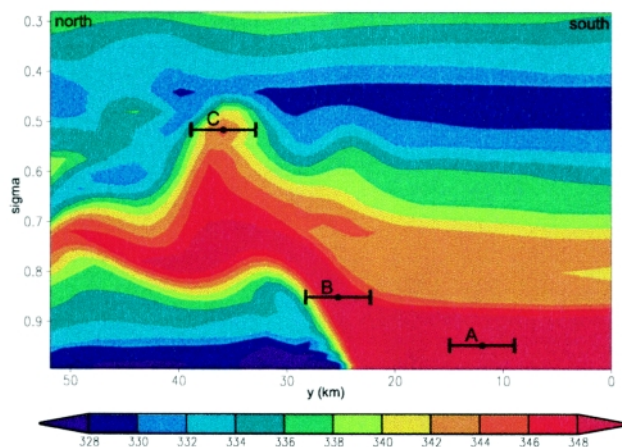


FIG. 20. North-south cross section of  $\theta_e$  (contour interval 2 K) at 1100 UTC, 6 Oct 1998. The bold bars depict distances of 3 km to the north and south of points A, B, and C. Temperature differences across these bars are listed in Table 4.

leading edge of convective systems observed during the GATE experiment.

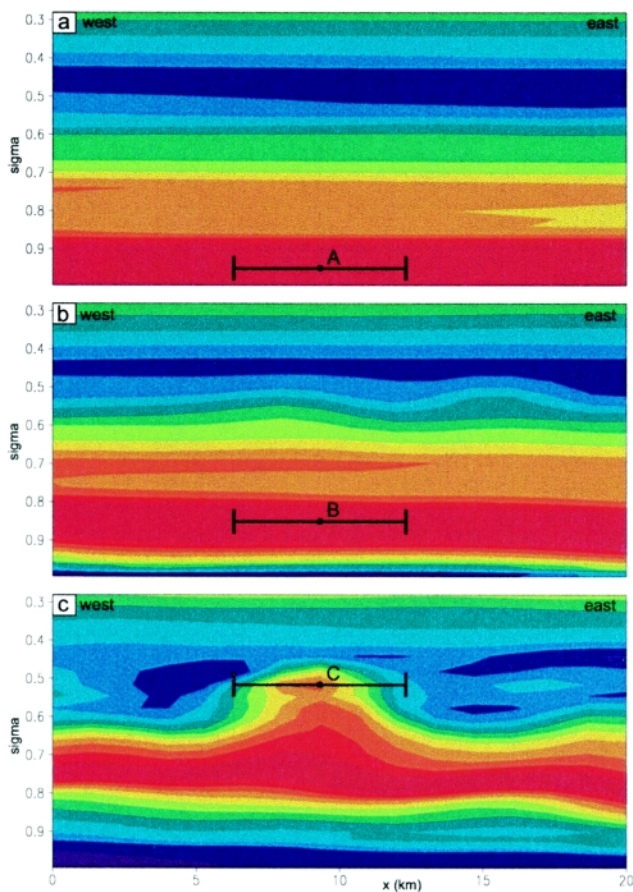


FIG. 21. Same as Fig. 20 except the cross sections are east-west and taken through points A, B, and C shown in Fig. 20.

## 6. Conclusions

Observations and numerical experiments indicate that a sixth static stability state, moist absolute instability, can occur in the low–midtroposphere. This stability state exists when the atmosphere creates and maintains a saturated environment with a lapse rate steeper than the moist-adiabatic lapse rate. This state is not simply a subset of one of the five other well-known states (Saucier 1955; Hess 1959), since it explicitly describes a saturated state, that is, it is not conditional upon saturation being achieved somehow—saturation *is* present. Observations and a numerical simulation show that a moist absolutely unstable state can exist in layers over 100 mb deep, can contiguously span distances of several hundred kilometers, and can persist for 30 min or more. The latter two of these properties are analogous to the dry absolutely unstable state.

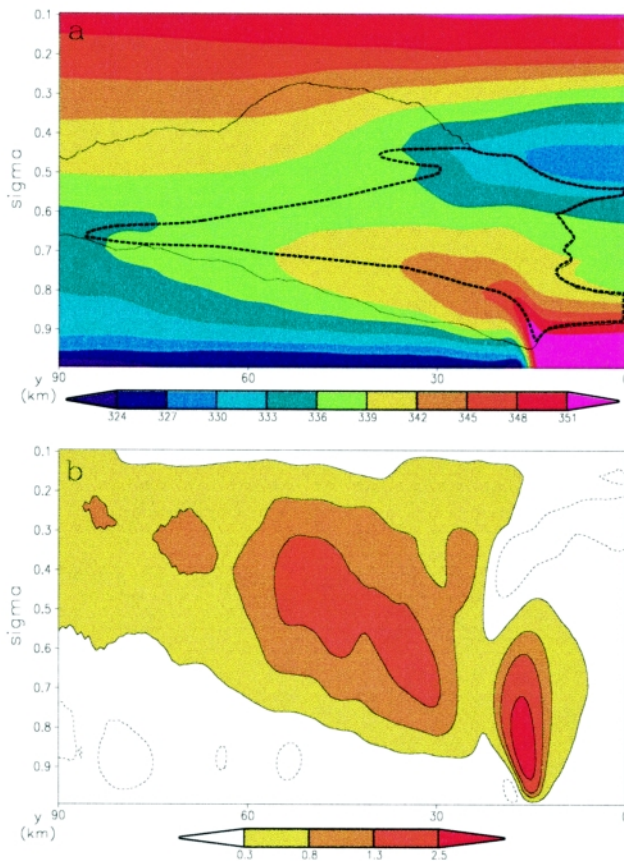


FIG. 22. Same as Fig. 19, except the fields are obtained by spatially and temporally averaging the model output (see text for details of averaging); in (a), the thin contour represents the  $0.1 \text{ g kg}^{-1}$  cloud water contour, and the thick contour outlines the MAUL, and; in (b), the dashed contours at  $-0.3 \text{ m s}^{-1}$  and the solid contours at  $+0.3, +0.8, +1.3$  and  $+2.5 \text{ m s}^{-1}$ .

Although the presence of moist absolutely unstable layers has been shown in other papers (e.g., Table 5), it usually is not acknowledged. In the few works that do recognize the existence of this static stability state, it seems to be construed as a fleeting condition removed nearly instantaneously by powerful buoyancy-forced overturning. However, it is argued here that, as a general principle, *a moist absolutely unstable layer can be maintained if the rate at which the unstable state is being created by mesoscale processes is greater than the rate at which it is being removed by cloud-scale turbulent overturning*. Such a rate imbalance is likely to exist in the inflow region of certain mesoscale convective systems where dynamically driven mesoscale ascent can rival or even exceed the vertical velocities produced by buoyancy.

It is important to recognize that ascent in the presence of moist absolute instability produces warming, not cooling. Therefore, the temperature difference between parcels and their environment is reduced, and parcel theory (which assumes a stationary environment) cannot be applied. Since actual buoyancy forces are reduced relative to that described by parcel theory, the spatial and temporal scales of moist absolute instability can be much larger than has been previously thought. The conventional view of deep cumulonimbus growth ensuing immediately after the creation of a MAUL does not adequately describe the processes.

Implications of the existence of MAULs on the conceptual model of MCSs were also presented. Viewing MCSs as vertically expanding slabs of moist, turbulent mixing helps explain several features of MCSs. In particular, the generation of mesoscale regions of saturation can be accomplished much more readily through this conceptual model than through an ensemble of discrete cumulonimbus towers. The existence of mesoscale regions of saturation has been used to help explain the generation of midlevel mesovortices, rear inflow jets, wake lows, etc., in MCSs (e.g., Johnson and Hamilton 1988; Chen and Frank 1993; Yu et al. 1999). Also, others have shown how the stratiform region is a large contributor to the surface-based cold pool/mesohigh (e.g., Zhang et al. 1994). Thus, we believe that MAULs play an integral part in determining MCS properties and behavior.

## 7. Concluding remarks

We recognize that what actually happens in slabs with moist absolutely unstable layers may depart from

TABLE 5. List of papers that contain figures with moist absolutely unstable layers.

Study	Figure	Method of observation
Davies-Jones and Henderson (1974)	Multiple figures in appendix A	Rawinsondes
Zipser et al. (1981)	Fig. 13	Rawinsonde
Rotunno et al. (1988)	Figs. 11, 12, and 14	Idealized numerical simulation
Crook and Moncrief (1988)	Fig. 9	Idealized numerical simulation
Colman (1990b)	Fig. 9	Rawinsonde
Ryan et al. (1992)	Fig. 14	Rawinsonde
Weisman (1992)	Fig. 6	Idealized numerical simulation
Yang and Houze (1995)	3a	Modified rawinsonde
Ziegler et al. (1997)	Fig. 18	Observed numerical simulation
Kain and Fritsch (1998)	Figs. 1, 3, and 10	Rawinsondes and simulation
Ziegler and Rasmussen (1998)	Fig. 18	Modified rawinsonde

the ideas presented here. Nevertheless, it is argued here that moist absolute instability is a basic state that forms in the developing stage of many MCSs and lasts throughout their mature stage. We hypothesize that moist absolute instability may be important in determining the internal structure of the convective system. It is conceivable that, just as the depth of the surface-based mixed layer strongly affects the size and number of dry eddies in the dry planetary boundary layer, the strength and depth of the moist absolutely unstable layer may affect the size and number of moist eddies. In other words, the properties (e.g., depth and intensity) of the moist absolutely unstable layer may help explain the variations in the cellular structure of the convective region of MCSs. A similar analogy between the dry planetary boundary layer and the moist layer of convective systems was proposed by Zipser and LeMone (1980).

Numerical simulations have given us the opportunity to inexpensively explore the structure of MAULs. However, high-resolution (both spatially and temporally) observations are needed to evaluate the performance of these numerical simulations. Given the rarity of past observations of MAULs, a specially designed field project appears to be necessary. Assuming the model-predicted MAUL structure is correct, special observational methods would be necessary to observe

its properties. For example, serial ascents of balloons from fixed locations ahead of an approaching MCS or dropsondes into the convective region might be an effective way to observe the three-dimensional structure of a MAUL. The use of airborne remote sensors or rocket-borne sensors could help solve the problem associated with horizontal drift of balloon-borne sensors. Or, successive aircraft penetrations of a MCS at multiple elevations would be insightful. Of course, the typical problems associated with measuring temperature and relative humidity in saturated conditions would have to be addressed.

We have performed additional numerical simulations to investigate the sensitivity of simulated MAUL structure to horizontal and vertical resolution, the representation of subgrid-scale turbulence, and different formulations of precipitation microphysics. In all our experiments, MAULs exist regardless of these changes. Since model grid spacings less than 4 km are partially resolving turbulent mixing, while at the same time the subgrid-scale turbulence parameterization is accounting for the same processes, it is possible that the simulations presented here are overcounting the effects of turbulent mixing. If this is true, then it further supports the existence and perpetuation of moist absolutely unstable layers, since turbulent mixing

should remove the unstable structure. The fact that turbulent mixing may be overdone in the simulations supports the assertion that forced mesoscale ascent can overwhelm turbulent mixing, thus maintaining the moist absolutely unstable layer.

Finally, as noted in section 2, it is likely that moist absolutely unstable layers are not restricted to just mesoscale convective systems. Stratocumulus layers (radiative cooling > turbulent mixing) seem to be able to support a moist absolutely unstable layer, albeit a much weaker structure than that produced by powerful mesoscale ascent in a conditionally unstable environment. It is also conceivable that the powerful mesoscale ascent observed in the eyewall region of tropical cyclones may produce moist absolutely unstable conditions in the lowest few hundred millibars. If this condition is eliminated in a manner similar to how it is eliminated in mesoscale convective systems, then it may be instrumental in the formation of the saturated, moist-adiabatic environment characteristic of this region. The main point remains, however, that a moist absolutely unstable layer will be supported wherever a mechanism for forced cooling and saturation is greater than the compensating rate of stabilization by buoyancy-driven accelerations and/or turbulent mixing.

*Acknowledgments.* The authors appreciate many helpful discussions with several people who shared their ideas and opinions on this topic. Their input has greatly strengthened the ideas presented here. We wish to acknowledge the valuable input from Jack Kain, Rob Rogers, Peter Bannon, George Young, John Clark, Bill Frank, Dave Stauffer, Nelson Seaman, John Wyngaard, and Bob Maddox. We also wish to acknowledge the constructive comments and suggestions from the reviewers: Brad Smull, Peggy LeMone, Doug Lilly, and an anonymous reviewer. Special thanks go to Bob Hart for endless help with programming and graphical presentation of model output, and to Phillip Spencer for reviewing the first draft of this paper. This work was supported by NSF Grant ATM 9806309 and NASA Grant NAG 5-2927.

## References

- Anthes, R. A., 1977: A cumulus parameterization scheme utilizing a one-dimensional cloud model. *Mon. Wea. Rev.*, **105**, 270–286.
- Arakawa, A., and W. H. Schubert, 1974: Interaction of a cumulus cloud ensemble with the large-scale environment, Part I. *J. Atmos. Sci.*, **31**, 674–701.
- Betts, A. K., R. W. Grover, and M. W. Moncrieff, 1976: Structure and motion of tropical squall-lines over Venezuela. *Quart. J. Roy. Meteor. Soc.*, **102**, 395–404.
- Biggerstaff, M. I., and R. A. Houze Jr., 1993: Kinematics and microphysics of the transition zone of the 10–11 June 1985 squall line. *J. Atmos. Sci.*, **50**, 3091–3110.
- Bjerknes, J., 1938: Saturated-adiabatic ascent of air through dry-adiabatically descending environment. *Quart. J. Roy. Meteor. Soc.*, **64**, 325–330.
- Blackmore, W. H., and B. Taubvurtzel, 1999: Environmental chamber tests of NWS rawinsonde relative humidity sensors. Preprints, *15th Int. Conf. on Interactive Information and Processing Systems*, Dallas, TX, Amer. Meteor. Soc., 259–262.
- Bluestein, H. B., and M. H. Jain, 1985: Formation of mesoscale lines of precipitation: Severe squall lines in Oklahoma during the spring. *J. Atmos. Sci.*, **42**, 1711–1732.
- Bolton, D., 1980: The computation of equivalent potential temperature. *Mon. Wea. Rev.*, **108**, 1046–1053.
- Byers, H. R., and R. R. Braham, 1948: Thunderstorm structure and circulation. *J. Meteor.*, **5**, 71–86.
- Chalon, J. P., G. Jaubert, F. Roux, and J. P. Lafore, 1988: The west African squall line observed on 23 June 1981 during COPT 81: Mesoscale structure and transports. *J. Atmos. Sci.*, **45**, 2744–2763.
- Chen, S. S., and W. M. Frank, 1993: A numerical study of the genesis of extratropical convective mesovortices. Part I: Evolution and dynamics. *J. Atmos. Sci.*, **50**, 2401–2426.
- Chong, M., P. Amayenc, G. Scialom, and J. Testud, 1987: A tropical squall line observed during the COPT 81 Experiment in West Africa. Part I: Kinematic structure inferred from dual-doppler radar data. *Mon. Wea. Rev.*, **115**, 670–694.
- Colman, B. R., 1990a: Thunderstorms above frontal surfaces in environments without positive CAPE. Part I: A climatology. *Mon. Wea. Rev.*, **118**, 1103–1121.
- , 1990b: Thunderstorms above frontal surfaces in environments without positive CAPE. Part II: Organization and instability mechanism. *Mon. Wea. Rev.*, **118**, 1123–1144.
- Cotton, W. R., M.-S. Lin, R. L. McAnelly, and C. J. Trembach, 1989: A composite model of mesoscale convective complexes. *Mon. Wea. Rev.*, **117**, 765–783.
- Crook, N. A., and M. W. Moncrieff, 1988: The effect of large-scale convergence on the generation and maintenance of deep moist convection. *J. Atmos. Sci.*, **45**, 3606–3624.
- Davies-Jones, R. P., and J. H. Henderson, 1974: Updraft properties deduced from rawinsondings. NOAA Tech. Memo. ERL NSSL-72, 117 pp.
- Droegemeier, K. K., and R. B. Wilhelmson, 1987: Numerical simulation of thunderstorm outflow dynamics. Part I: Outflow sensitivity experiments and turbulence dynamics. *J. Atmos. Sci.*, **44**, 1180–1210.
- Dudhia, J., 1993: A nonhydrostatic version of the Penn State-NCAR mesoscale model: Validation tests and simulation of an Atlantic cyclone and cold front. *Mon. Wea. Rev.*, **121**, 1493–1513.
- , and W. M. Moncrieff, 1987: A numerical simulation of quasi-stationary tropical convection bands. *Quart. J. Roy. Meteor. Soc.*, **113**, 929–967.
- Emanuel, K. A., 1997: Overview of atmospheric convection. *The Physics and Parameterization of Moist Atmospheric Convection*, R. K. Smith, Ed., Kluwer Academic Publishers, 1–28.
- Fovell, R. G., and Y. Ogura, 1988: Numerical simulation of a mid-latitude squall line in two dimensions. *J. Atmos. Sci.*, **45**, 3846–3880.

- Frankhauser, J. C., G. M. Barnes, and M. A. LeMone, 1992: Structure of a midlatitude squall line formed in strong unidirectional shear. *Mon. Wea. Rev.*, **120**, 237–260.
- Fujita, T. T., 1955: Results of detailed synoptic studies of squall lines. *Tellus*, **4**, 405–436.
- Gamache, J. F., and R. A. Houze Jr., 1982: Mesoscale air motions associated with a tropical squall line. *Mon. Wea. Rev.*, **110**, 118–135.
- Hane, C. E., 1986: Extratropical squall lines and rainbands. *Mesoscale Meteorology and Forecasting*, P. Ray, Ed., Amer. Meteor. Soc., 359–389.
- Hess, S. L., 1959: *Introduction to Theoretical Meteorology*. Holt, 362 pp.
- Heymsfield, G. M., and S. Schotz, 1985: Structure and evolution of a severe squall line over Oklahoma. *Mon. Wea. Rev.*, **113**, 1563–1589.
- Hildebrand, P. H., and Coauthors, 1996: The ELDORA/ASTRAIA airborne Doppler weather radar: High-resolution observations from TOGA COARE. *Bull. Amer. Meteor. Soc.*, **77**, 213–232.
- Hodge, M. W., 1956: Superadiabatic lapse rates of temperature in radiosonde observations. *Mon. Wea. Rev.*, **84**, 103–106.
- Houze, R. A., 1977: Structure and dynamics of a tropical squall-line system. *Mon. Wea. Rev.*, **105**, 1540–1567.
- , S. A. Rutledge, M. I. Biggerstaff, and B. F. Smull, 1989: Interpretation of Doppler weather radar displays of midlatitude mesoscale convective systems. *Bull. Amer. Meteor. Soc.*, **70**, 608–619.
- , B. F. Smull, and P. Dodge, 1990: Mesoscale organization of springtime rainstorms in Oklahoma. *Mon. Wea. Rev.*, **118**, 613–654.
- Johnson, R. H., and P. J. Hamilton, 1988: The relationship of surface pressure features to the precipitation and air flow structure of an intense midlatitude squall line. *Mon. Wea. Rev.*, **116**, 1444–1472.
- Jorgensen, D. P., M. A. LeMone, and S. B. Trier, 1997: Structure and evolution of the 22 February 1993 TOGA COARE squall line: Aircraft observations of precipitation, circulation, and surface energy fluxes. *J. Atmos. Sci.*, **54**, 1961–1985.
- Kain, J. S., and J. M. Fritsch, 1990: A one-dimensional entraining/detraining plume model. *J. Atmos. Sci.*, **47**, 2784–2802.
- , and ———, 1998: Multiscale convective overturning in mesoscale convective systems: Reconciling observations, simulations, and theory. *Mon. Wea. Rev.*, **126**, 2254–2273.
- Kingsmill, D. E., and R. A. Houze Jr., 1999: Kinematic characteristics of air flowing into and out of precipitating convection over the West Pacific warm pool: An airborne Doppler radar survey. *Quart. J. Roy. Meteor. Soc.*, **125**, 1165–1207.
- Lafore, J. P., J. L. Redelsperger, and G. Jaubert, 1988: Comparison between a three-dimensional simulation and Doppler radar data of a tropical squall line: Transports of mass, momentum, heat, and moisture. *J. Atmos. Sci.*, **45**, 3483–3500.
- Leary, C. A., 1980: Temperature and humidity profiles in mesoscale unsaturated downdrafts. *J. Atmos. Sci.*, **37**, 1005–1012.
- , and R. A. Houze, 1979: The structure and evolution of convection in a tropical cloud cluster. *J. Atmos. Sci.*, **36**, 437–457.
- , and E. N. Rappaport, 1987: The life cycle and internal structure of a mesoscale convective complex. *Mon. Wea. Rev.*, **115**, 1503–1527.
- LeMone, M. A., and E. J. Zipser, 1980: Cumulonimbus vertical velocity events in GATE. Part I: Diameter, intensity, and mass flux. *J. Atmos. Sci.*, **37**, 2444–2457.
- , and D. P. Jorgensen, 1991: Precipitation and kinematic structure of an oceanic mesoscale convective system. Part II: Momentum transport and generation. *Mon. Wea. Rev.*, **119**, 2638–2653.
- , and M. W. Moncrieff, 1994: Momentum and mass transport by convective bands: Comparisons of highly idealized dynamical models to observations. *J. Atmos. Sci.*, **51**, 281–305.
- , G. M. Barnes, E. J. Szoke, and E. J. Zipser, 1984: The tilt of the leading edge of mesoscale tropical convective lines. *Mon. Wea. Rev.*, **112**, 510–519.
- Lehrer, S. M., and R. H. Johnson, 1995: Surface pressure and precipitation life cycle characteristics of PRE-STORM mesoscale convective systems. *Mon. Wea. Rev.*, **123**, 600–621.
- Lilly, D. K., 1960: On the theory of disturbances in a conditionally unstable atmosphere. *Mon. Wea. Rev.*, **88**, 1–17.
- Liu, Y., D.-L. Zhang, and M. K. Yau, 1997: A multiscale numerical study of Hurricane Andrew (1992). Part I: Explicit simulation and verification. *Mon. Wea. Rev.*, **125**, 3073–3093.
- Lucas, C., E. J. Zipser, and M. A. LeMone, 1994a: Vertical velocity in oceanic convection off tropical Australia. *J. Atmos. Sci.*, **51**, 3183–3193.
- , ———, and ———, 1994b: Convective available potential energy in the environment of oceanic and continental clouds: Correction and comments. *J. Atmos. Sci.*, **51**, 3829–3830.
- Maddox, R. A., 1983: Large-scale meteorological conditions associated with midlatitude mesoscale convective complexes. *Mon. Wea. Rev.*, **111**, 1475–1493.
- McAnelly, R. L., and W. R. Cotton, 1986: Meso- $\beta$ -scale characteristics of an episode of meso- $\alpha$ -scale convective complexes. *Mon. Wea. Rev.*, **114**, 1740–1770.
- Moncrieff, M. W., 1981: A theory of organized steady convection and its transport properties. *Quart. J. Roy. Meteor. Soc.*, **107**, 29–50.
- , 1989: Analytical models of narrow cold-frontal rainbands and related phenomena. *J. Atmos. Sci.*, **46**, 150–162.
- Moncrieff, M. W., and J. S. Green, 1972: The propagation and transfer properties of steady convective overturning in shear. *Quart. J. Roy. Meteor. Soc.*, **98**, 336–352.
- Newton, C. W., 1950: Structure and mechanism of the prefrontal squall line. *J. Meteor.*, **7**, 210–222.
- , and H. R. Newton, 1959: Dynamical interactions between large convective clouds and environment with vertical shear. *J. Meteor.*, **16**, 483–496.
- Ogura, Y., and Y. Chen, 1977: A life history of an intense mesoscale convective storm in Oklahoma. *J. Atmos. Sci.*, **34**, 1458–1476.
- , and M. T. Liou, 1980: The structure of a midlatitude squall line: A case study. *J. Atmos. Sci.*, **37**, 553–567.
- Pandya, R. E., and D. R. Durran, 1996: The influence of convectively generated thermal forcing on the mesoscale circulation around squall lines. *J. Atmos. Sci.*, **53**, 2924–2951.
- Reisner, J. R., M. Rasmussen, and R. T. Bruintjes, 1998: Explicit forecasting of supercooled liquid water in winter storms using the MM5 mesoscale model. *Quart. J. Roy. Meteor. Soc.*, **124B**, 1071–1107.
- Riehl, H., and J. Malkus, 1958: On the heat balance in the equatorial trough zone. *Geophysica*, **6**, 503–538.

- Rotunno, R., J. B. Klemp, and M. L. Weisman, 1988: A theory for strong, long-lived squall lines. *J. Atmos. Sci.*, **45**, 463–485.
- Roux, F., 1988: The west African squall line observed on 23 June 1981 during COPT 81: Kinematics and thermodynamics of the convective region. *J. Atmos. Sci.*, **45**, 406–426.
- , J. Testud, M. Payen, and B. Pinty, 1984: West African squall-line thermodynamic structure retrieved from dual-Doppler radar observations. *J. Atmos. Sci.*, **41**, 3104–3121.
- Ryan, B. F., G. M. Barnes, and E. J. Zipser, 1992: A wide rainbank in a developing tropical cyclone. *Mon. Wea. Rev.*, **120**, 431–447.
- Saucier, W. J., 1955: *Principles of Meteorological Analysis*. Dover, 438 pp.
- Schmidlin, F. J., 1998: Radiosonde relative humidity sensor performance: The WMO intercomparison—September 1995. Preprints, *10th Symp. on Meteorological Observations and Instrumentation*. Phoenix, AZ, Amer. Meteor. Soc., 68–71.
- Seman, C. J., 1994: A numerical study of nonlinear nonhydrostatic conditional symmetric instability in a convectively unstable atmosphere. *J. Atmos. Sci.*, **51**, 1352–1371.
- Skamarock, W. C., 1994: MM5 and cloud model simulations of supercell thunderstorms. Preprints, *The Fourth PSU/NCAR Mesoscale Model Users' Workshop*. Boulder, CO, National Center for Atmospheric Research, 11–14.
- , M. L. Weisman, and J. B. Klemp, 1994: Three-dimensional evolution of simulated long-lived squall lines. *J. Atmos. Sci.*, **51**, 2563–2584.
- Slonaker, R. L., B. E. Schwartz, and W. J. Emery, 1996: Occurrence of nonsurface superadiabatic lapse rates within RAOB data. *Wea. Forecasting*, **11**, 350–359.
- Smull, B. F., and R. A. Houze, 1985: A midlatitude squall line with a trailing region of stratiform rain: Radar and satellite observations. *Mon. Wea. Rev.*, **113**, 117–133.
- , and ———, 1987: Dual-Doppler radar analysis of a midlatitude squall line with a trailing region of stratiform rain. *J. Atmos. Sci.*, **44**, 2128–2148.
- , and J. A. Augustine, 1993: Multiscale analysis of a mature mesoscale convective complex. *Mon. Wea. Rev.*, **121**, 103–132.
- Srivastava, R. C., T. J. Matejka, and T. J. Lorello, 1986: Doppler radar study of the trailing anvil region associated with a squall line. *J. Atmos. Sci.*, **43**, 356–377.
- Thorpe, A. J., M. J. Miller, and M. W. Moncrieff, 1982: Two-dimensional convection in non-constant shear: A model of mid-latitude squall lines. *Quart. J. Roy. Meteor. Soc.*, **108**, 739–762.
- Trier, S. B., and E. B. Parsons, 1993: Evolution of environmental conditions preceding the development of a nocturnal mesoscale convective complex. *Mon. Wea. Rev.*, **121**, 1078–1098.
- Weisman, M. L., 1992: The role of convectively generated rear-inflow jets in the evolution of long-lived mesoconvective systems. *J. Atmos. Sci.*, **49**, 1826–1847.
- , J. B. Klemp, and R. Rotunno, 1988: Structure and evolution of numerically simulated squall lines. *J. Atmos. Sci.*, **45**, 1990–2013.
- , W. C. Skamarock, and J. B. Klemp, 1997: The resolution dependence of explicitly modeled convective systems. *Mon. Wea. Rev.*, **125**, 527–548.
- World Meteorological Organization, 1996: Guide to meteorological instruments and methods of observations. 6th ed. WMO.
- Yang, M.-J., and R. A. Houze Jr., 1995: Multicell squall-line structure as a manifestation of vertically trapped gravity waves. *Mon. Wea. Rev.*, **123**, 641–661.
- Young, G. S., and J. M. Fritsch, 1989: A proposal for general conventions in analyses of mesoscale boundaries. *Bull. Amer. Meteor. Soc.*, **70**, 1412–1421.
- Yu, C.-K., B. J.-D. Jou, and B. F. Smull, 1999: Formative stage of a long-lived mesoscale vortex observed by airborne Doppler radar. *Mon. Wea. Rev.*, **127**, 838–857.
- Yuter, S. E., and R. A. Houze, 1995a: Three-dimensional kinematic and microphysical evolution of Florida cumulonimbus. Part I: Spatial distribution of updrafts, downdrafts, and precipitation. *Mon. Wea. Rev.*, **123**, 1921–1940.
- , and ———, 1995b: Three-dimensional kinematic and microphysical evolution of Florida cumulonimbus. Part II: Frequency distributions of vertical velocity, reflectivity, and differential reflectivity. *Mon. Wea. Rev.*, **123**, 1941–1963.
- Zhang, D.-L., K. Gao, and D. B. Parsons, 1989: Numerical simulation of an intense squall line during 10–11 June 1985 PRE-STORM. Part I: Model verification.
- , J. S. Kain, J. M. Fritsch, and K. Gao, 1994: Comments on “Parameterization of convective precipitation in mesoscale numerical models: A critical review.” *Mon. Wea. Rev.*, **122**, 2222–2231.
- Ziegler, C. L., and E. N. Rasmussen, 1998: The initiation of moist convection at the dryline: Forecasting issues from a case study perspective. *Wea. Forecasting*, **13**, 1106–1131.
- , T. J. Lee, and R. A. Pielke, 1997: Convective initiation at the dryline: A modeling study. *Mon. Wea. Rev.*, **125**, 1001–1026.
- Zipser, E. J., 1977: Mesoscale and convective-scale downdrafts as distinct components of squall-line circulation. *Mon. Wea. Rev.*, **105**, 1568–1589.
- , and M. A. LeMone 1980: Cumulonimbus vertical velocity events in GATE. Part II: Synthesis and model core structure. *J. Atmos. Sci.*, **37**, 2458–2469.
- , R. J. Meitin, and M. A. LeMone, 1981: Mesoscale motion fields associated with a slowly moving GATE convective band. *J. Atmos. Sci.*, **38**, 1725–1750.
- , Y.-L. Chen, and E. J. Szoke, 1983: On the generation of heavy precipitation within the anvil system of a tropical squall line. Preprints, *21st Amer. Meteor. Soc. Conf. on Radar Meteorology*, Edmonton, AB, Canada, Amer. Meteor. Soc., 50–56.

